JOURNAL OF PETROLOGY | VOLUME 38 | NUMBER 8 | PAGES 1047–1074 | 1997

Mantle Melting and Melt Extraction Processes beneath Ocean Ridges: Evidence from Abyssal Peridotites

YAOLING NIU*

DEPARTMENT OF EARTH SCIENCES, THE UNIVERSITY OF QUEENSLAND, BRISBANE, QLD. 4072, AUSTRALIA

RECEIVED JANUARY 22, 1996 REVISED TYPESCRIPT ACCEPTED APRIL 8, 1997

This paper presents the results of the first quantitative petrological modelling of abyssal peridotites. The mantle beneath a ridge may be considered as two regions: (1) the melting region between the solidus (P_o) at which upwelling mantle begins to melt, and the depth (P_f) at which melting stops because of conductive cooling to the surface; (2) the thermal boundary layer between P_f and the base of crust. In the melting region, decompression near-fractional melting is characterized by the reaction $aCpx + bOpx + cSpl = dOl + 1Melt$, *i.e. clinopyroxene, orthopyroxene and spinel melt whereas olivine crystallizes as melting proceeds. In much of the pressure range ($P_o \leq 25$ kbar), orthopyroxene contributes more than clinopyroxene to the melt (i.e.* $b>a$*) during decompression melting, which is unexpected from isobaric melting experiments, but is constrained by the incongruent melting of* $Opx \Rightarrow Ol + SiO_2$ *with decreasing pressure. The melting reaction also explains the so-called local trend of mid-ocean ridge basalt (MORB) chemistry characteristic of slow-spreading ridges. Melts produced over a wide region and depth range in the mantle will ascend and migrate laterally towards the axial zone of crustal accretion. These melts cool and crystallize olivine as they pass through previously depleted residues in the thermal boundary layer. This explains why abyssal peridotites have excess olivine relative to simple melting residues. The greater the ambient extent of mantle melting, the more melt is produced in the mantle. Thus, greater extents of melting lead to more olivine (up to 50% of the rock mass in abyssal peridotites) crystallization at shallow levels. Additional important implications are: (1) neither MORB melts nor the bulk igneous crust is compositionally comparable with partial melts produced in peridotite melting experiments because primary mantle melts crystallize olivine back in the mantle; (2) diffusive porous flow is the primary mode of melt migration even at very shallow levels because excess olivine is observed on thin-section scales in abyssal peridotites; (3) low-pressure melt equilibration during ascent is inevitable because the melting reaction preserved in residual peridotites requires continuous solid–liquid equilibration, and because olivine crystallization in the thermal boundary layer is the natural consequence of melt ascent and cooling; (4) perfect fractional melting is unlikely because melt porosity (a few percent?) in the melting mantle is required by the melting reaction, whole-rock major element data and other observations; (5) compositional variations of both MORB and abyssal peridotites are consistent with varying extents (~10–22%) of mantle melting beneath global ocean ridges.*

KEY WORDS: *abyssal peridotites; MORB; petrogenesis; mantle melting; melt extraction; mid-ocean ridges; ridge dynamics*

INTRODUCTION

Plate separation at ocean ridges causes the mantle beneath to ascend. This ascent results in pressure-release partial melting of the mantle material (e.g. Bottinga & Allègre, 1973, 1978; Carmichael *et al.*, 1974; Oxburgh, 1980). The melts so produced, when extracted, build the ocean crust with complementary residue remaining in the lithospheric mantle. Mid-ocean ridge basalts (MORBs) that form the uppermost layer of the ocean crust are considered to represent the final product of these melts that have evolved primarily through fractional crystallization as a result of cooling at shallow levels (e.g. O'Hara, 1968*a*; Walker *et al.*, 1979; Sinton & Detrick, 1992), whereas abyssal peridotites are thought to be the residues that have been tectonically exposed on the

*Telephone: 61-7-3365-2372. Fax: 61-7-3365-1277. e-mail: niu@earthsciences.uq.edu.au

seafloor (e.g. Dick & Fisher, 1984; Dick *et al.*, 1984; Nicolas, 1989), mostly along fracture zones and within transforms (e.g. Prinz *et al.*, 1976; Hamlyn & Bonatti, 1980; Dick *et al.*, 1984; Dick, 1989; Hékinian *et al.*, 1992, 1993). Although this simple concept of melt generation and ocean crust formation as an integral part of the plate tectonics theory has long been accepted, important aspects such as the extent and depth of melting, melt segregation, melt–solid interactions, and the mechanisms of melt focusing towards the very narrow (<1–2 km) axial zone of crust accretion have been the subjects of much research in recent years in areas of marine geology, geophysics and petrology [see reviews by Forsyth (1992), Langmuir *et al.* (1992) and Turcotte & Phipps Morgan (1992)].

Petrological studies have been particularly important. For example, Dick and co-workers (e.g. Dick & Fisher, 1984; Dick *et al.*, 1984; Michael & Bonatti, 1985; Johnson *et al.*, 1990) showed that abyssal peridotites and spatially associated MORB exhibit correlated compositional variations that are consistent with varying extents of mantle melting. The relative extent of melting is high beneath hotspot-influenced shallow ridges, and is low beneath deep ridges away from hotspots (Dick *et al.*, 1984; Michael & Bonatti, 1985). These results have led to the recognition of global correlations of MORB chemistry with ridge axial depth and crustal thickness (Klein & Langmuir, 1987), and to the conjecture that mantle temperature variation exerts the primary control on the extent of mantle melting beneath ocean ridges (Dick *et al.*, 1984; Klein & Langmuir, 1987; McKenzie & Bickle, 1988; Niu & Batiza, 1991*a*; Langmuir *et al.*, 1992). On the other hand, Niu & Hékinian (1997*a*) showed that abyssal peridotites and MORB both consistently suggest that the extent of mantle melting beneath normal ocean ridges (thermally unaffected by hotspots) increases with increasing spreading rate. This new observation is in accord with the model predictions (e.g. Bottinga & Allègre, 1978; Reid & Jackson, 1981; Phipps Morgan & Forsyth, 1988; Chen & Morgan, 1990; Chen, 1996), and supports the notion that ocean ridges are mostly passive (McKenzie, 1967; Morgan, 1975; Parsons & Sclater, 1977; McKenzie & Bickle, 1988).

Regardless of whether the elevated extents of melting beneath a ridge result from fast spreading rates (e.g. the East Pacific Rise) or from a hotter mantle influenced by hotspots (e.g. the Mid-Atlantic Ridge near Azores hotspot), the observed variation in extent of melting accounts qualitatively well for the compositional complementarity between MORB and abyssal peridotites (Dick *et al.*, 1984; Niu & Hékinian, 1997*a*, 1997*b*; Niu *et al.*, 1997). Although these first-order observations are robust, many aspects of melting and melt extraction processes are not well understood, and important issues remain controversial. For example, Klein & Langmuir (1987) showed that globally, MORB displayed an inverse Fe_8–Na_8 (i.e. FeO and Na_2O corrected to an MgO = 8 wt % to remove fractionation effect) correlation, or global trend (Klein & Langmuir, 1989). These workers and others (e.g. Niu & Batiza, 1991*a*, 1993; Kinzler & Grove, 1992; Langmuir *et al.*, 1992) interpreted this correlation in terms of polybaric column melting models as reflecting mantle temperature variation. Others (e.g. Natland, 1989; Albarède, 1992; Shen & Forsyth, 1995), however, argued that the global trend may result from fertile mantle source compositional variations. Another major debate concerns the origin of a positive Fe_8–Na_8 correlation, or local trend (Klein & Langmuir, 1989), which is found to be characteristic of slow-spreading ridges (Niu & Batiza, 1993, 1994). Klein & Langmuir (1989) interpreted the local trend as resulting from melt extraction from different parts of a single melting column, i.e. melt extracted from the lower part of the column has a signature of high pressure (high Fe_8) and low degree (high Na_8) of melting, whereas melt extracted from the upper part of the column has a signature of low pressure (low Fe_8) and high degree (low Na_8) of melting. Kinzler & Grove (1992), however, argued that the local trend results from high-pressure fractional crystallization, whereas Niu & Batiza (1993, 1994) showed that the local trend can be explained by the decompression melting reaction (Pyroxene + Melt A⇒Olivine + Melt B) that is taking place in an ascending and melting mantle.

Historical debate over the melting pressure and composition of primary magmas parental to MORB was based largely on interpretations of isobaric experimental batch melts and on the use of simplified phase diagrams [see reviews by Elthon (1989) and Baker & Stolper (1994)]. Although the definition of primary magma needs revision given the polybaric, not isobaric, melting processes beneath ridges, the depth range and actual amounts of melting remain controversial (Langmuir *et al.*, 1992; Forsyth, 1993; Kinzler & Grove, 1993; Niu & Batiza, 1994; Plank *et al.*, 1995; Niu *et al.*, 1996). Controversies also exist on the melt porosity and the level and physical mechanisms of melt segregation in the melting mantle [see reviews by Forsyth (1992) and Turcotte & Phipps Morgan (1992)]. A related key question concerns the efficiency of melt extraction. Recent studies (e.g. Salters & Hart, 1989; Langmuir *et al.*, 1992) suggest that melts formed at depths in the mantle must be extracted rapidly without experiencing low-pressure equilibration during ascent. It is unclear, however, how low-pressure equilibration can be avoided if melts ascend by porous flow (e.g. McKenzie, 1984; Lundstrom *et al.*, 1994, 1995; Niu & Hékinian, 1997*b*).

To answer these questions and many others, quantitative understanding of abyssal peridotite genesis is primarily important. This is because abyssal peridotites record the entire history of melting, melt segregation,

melt migration, melt–solid interaction, and mantle flow before being tectonically exposed on the seafloor. However, abyssal peridotites have not been quantitatively modelled to the same extent as MORB (e.g. McKenzie & Bickle, 1988; Niu & Batiza, 1991*a*; Kinzler & Grove, 1992; Langmuir *et al.*, 1992). Since the pioneering work of Dick and co-workers, more recent studies of abyssal peridotite data include those by Elthon (1992) and Niu *et al.* (1997). Elthon (1992) interpreted the abyssal peridotites as being not simple residues, but modified by melt refertilization, whereas Niu *et al.* (1997) showed qualitatively that abyssal peridotites are not simple melting residues, but possess excess olivine. In this paper, I present the detailed analysis of these abyssal peridotite data in terms of mass balance calculations and phase equilibrium considerations. The results offer a better understanding of mantle melting and melt extraction processes beneath ocean ridges. I primarily concentrate on mineral modes and reconstructed whole-rock compositions of abyssal peridotites studied by Dick and co-workers (i.e. Dick, 1989; Johnson *et al.*, 1990; Johnson & Dick, 1992; Snow & Dick, 1995). The reader is referred to Niu *et al.* (1997) for data selection, procedures for bulk-rock composition reconstruction, and related discussions.

DATA AND MODEL INTERPRETATIONS

Abyssal peridotite whole-rock compositional systematics

In this section, I show that whole-rock compositions of abyssal peridotites define trends that are inconsistent with simple melting trends but consistent with the inference that the peridotites are residues with excess olivine.

Simple melting residues: model results

Figure 1 shows on MgO variation diagrams the major element compositions of simple residues calculated using the method of Niu & Batiza (1991*a*), modified by incorporating recent experimental data (Hirose & Kushiro, 1993; Baker & Stolper, 1994) (Appendix A; hereafter mNB91). The preferred fertile mantle composition used is detailed in Appendix B. Simple residues calculated by polybaric fractional melting beginning at two initial pressures (P_o = 15 and 25 kbar), and by isobaric batch melting at two pressures (P = 10 and 20 kbar) are broadly similar, but differ in detail. The systematics of all these oxides with respect to MgO are expected given their bulk distribution coefficients as a function of pressure and the extent of melting. It should be noted that FeO either increases or decreases with pressure, models and MgO, but the overall variation range is rather small because the bulk distribution coefficient of FeO correlates inversely with pressure, and is close to unity (Niu & Batiza, 1991*a*).

Abyssal peridotites: not simple residues

Figure 2 compares bulk compositions of abyssal peridotites with calculated residues (Fig. 1). Despite the scatter, abyssal peridotite data define trends on all these plots, although these are not all consistent with melting. The Al_2O_3–MgO and CaO–MgO trends are broadly similar to melting curves. The TiO_2–MgO and Na_2O–MgO trends are parallel to and closer to batch melting curves than fractional melting curves, although most data points plot above the batch melting curves. The higher than expected Na_2O abundances at a given MgO value were the primary evidence that led Elthon (1992) to argue that abyssal peridotites are not simple residues, but refertilized by a melt component. The trends on SiO_2–MgO and FeO–MgO plots clearly differ from melting curves by either model at any pressure. The steepness of the positive FeO–MgO correlation, in particular, contrasts with melting curves. Niu *et al.* (1997) have shown that residues produced by other existing melting models (Kinzler & Grove, 1992; Langmuir *et al.*, 1992) are essentially the same as those by mNB91, and have very flat FeO–MgO patterns. Varying fertile source compositions will only result in slight changes in the positions, but not slopes, of the model residues on these diagrams (see Niu *et al.*, 1997). Therefore, abyssal peridotites are not considered as simple residues.

Abyssal peridotites: mixtures of simple residues and excess olivine

An important aspect in Fig. 2 is the more or less linear trends on all the plots, suggesting mixing relationships. The depleted mixing endmember has high MgO, high FeO, low SiO_2, and no TiO_2, Al_2O_3, CaO and Na_2O. An obvious candidate for such an endmember is olivine. Indeed, as shown in Fig. 3, many abyssal peridotites have very high modal olivine, significantly higher than predicted for melting residues beneath ocean ridges. It is also clear from Fig. 3 that SiO_2, FeO and MgO abundances in bulk abyssal peridotites are largely controlled by mineral modes, particularly olivine modes, in these peridotites. Figure 4 shows the mean composition of abyssal peridotite olivine on SiO_2–MgO and FeO–MgO diagrams. Mixing lines between such an olivine and the model melting curves account well for the abyssal peridotite data. Olivine addition increases FeO and MgO and decreases SiO_2 in the bulk rock. The dashed lines enclose fields that result from mixing of olivine with diverse residues produced by melting a uniform source. The data suggest that abyssal peridotites are mixtures of simple residues and excess olivine.

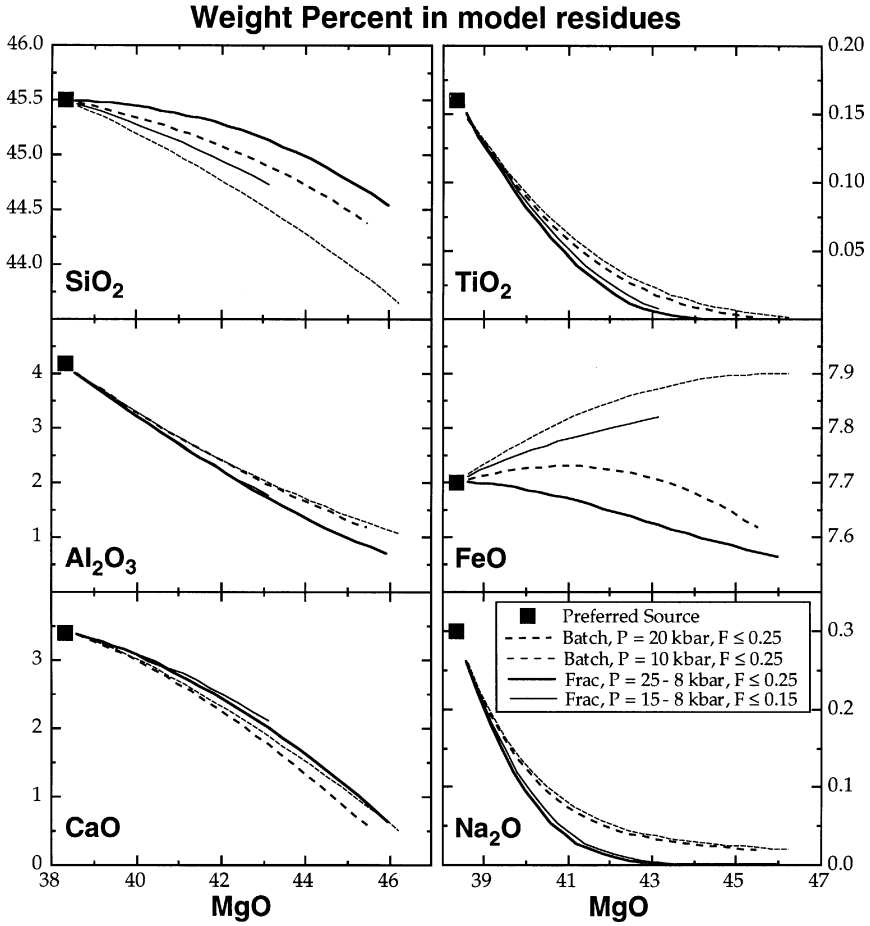

Fig. 1. MgO variation diagrams of SiO_2, TiO_2, Al_2O_3, FeO, CaO and Na_2O of simple melting residues calculated by models of polybaric near-fractional (1% melt porosity) melting with initial melting depths of $P_o = 15$ and 25 kbar, and of isobaric batch melting at $P = 10$ and 20 kbar using mNB91 (see Appendix A). The preferred source composition used is given in Appendix B.

As olivine effectively contains no TiO_2, Al_2O_3, CaO and Na_2O, addition of olivine dilutes the abundances of these elements in the bulk rock, but does not affect the melting signatures preserved. The systematics of these elements when plotted against MgO (Fig. 2) thus suggests that olivine addition is not a random process, but that the amount of olivine added increases with the overall extent of melting–depletion (Niu *et al.*, 1997; also see below).

A quantitative approach

It has long been recognized that compositions of partial melts produced by peridotite melting experiments depend on pressure and temperature (e.g. Green & Ringwood, 1967; Ito & Kennedy, 1967; O'Hara, 1968*b*; Stolper, 1980; Jaques & Green, 1980). This indicates that proportions of peridotite minerals entering melt during melting vary with pressure and temperature. In multiphase systems, melting is not eutectic, but is associated with peritectic reactions (Mysen, 1979; Presnall *et al.*, 1979). Significant progress has been made in recent years in quantifying the melting reactions, in either simplified or multi-component natural systems, under conditions appropriate for melting beneath ocean ridges (Kinzler & Grove, 1992; Baker & Stolper; 1994; Walter & Presnall, 1994; Walter *et al.*, 1995). Application of these results is, however, not straightforward, because experiments are conducted isobarically, whereas pressure-release melting in response to plate separation beneath ocean ridges is polybaric.

O'Hara (1968*b*) was, perhaps, one of the first advocates for polybaric processes in interpreting mafic magma genesis using phase equilibria, and Jamieson (1970) may be the first who attempted to infer polybaric paths of mafic magma evolution. Quantitative polybaric models have not been available until very recent years (e.g. Klein & Langmuir, 1987; McKenzie & Bickle, 1988; Niu &

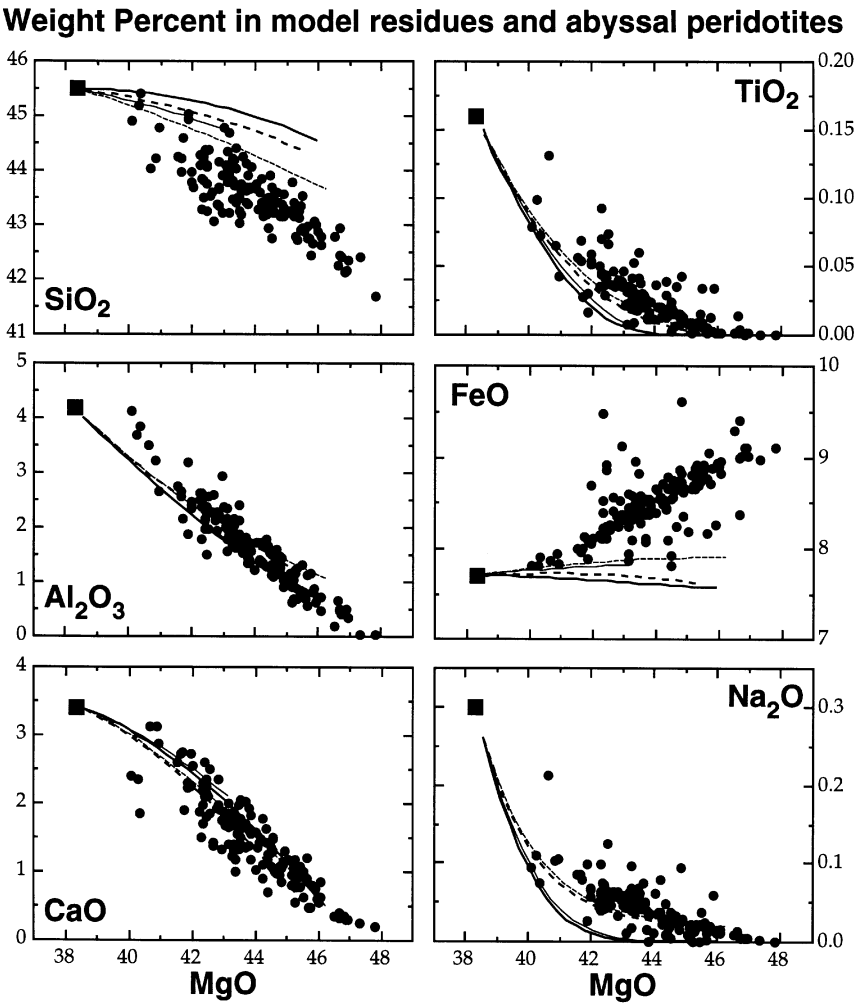

Fig. 2. MgO variation diagrams of SiO_2, TiO_2, Al_2O_3, FeO, CaO and Na_2O of the reconstructed bulk abyssal peridotite compositions (Niu *et al.*, 1997). For comparison, calculated model residues (as in Fig. 1) also are shown. It should be noted that at a given MgO value, Na_2O and TiO_2 abundances are higher than calculated in residues, but closer to batch melting than fractional melting. Importantly, SiO_2 is significantly lower, and FeO is significantly higher than expected for simple residues by either model. The positive MgO–FeO correlation is totally unexpected, indicating that abyssal peridotites are not simple residues.

Batiza, 1991*a*; Kinzler & Grove, 1992; Langmuir *et al.*, 1992), but these only deal with basaltic melts. There has been no attempt to model melting residues or abyssal peridotites. One of the major difficulties is the lack of a sound thermodynamic means for evaluating both proportions and compositions of residual minerals from a given bulk composition as a function of temperature and pressure (see Wood, 1987). Previous attempts at estimating residual mineral modes and compositions from melting models include those by Bickle (1986) and Niu & Batiza (1991*b*), but these were aimed only at evaluating melt-depletion induced buoyancy.

Here I take a simple forward modelling approach, which includes: (1) calculating bulk compositions of residues produced by polybaric near-fractional melting using mNB91; (2) determining the residual mineral modes by a simple norm–mode conversion; (3) examining the systematics of residual modes as a function of the extent of melting and initial melting pressures; (4) comparing the model results with abyssal peridotites.

Using normative mineralogy

The conventional CIPW norm scheme calculates Ab, An, Di, Hy and Ol, which describe >99% total mass of both abyssal peridotites and model melting residues. These normative minerals are converted to a normative assemblage relevant to peridotites and model melting residues: olivine (*ol*), orthopyroxene (*opx*) and clinopyroxene (*cpx*) (see Appendix C). It should be noted that

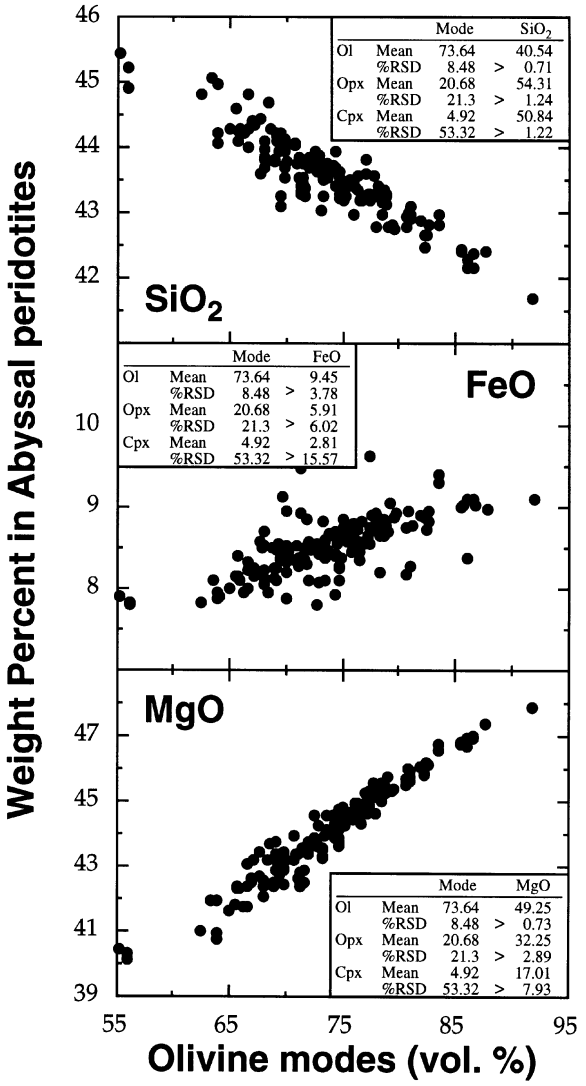

Fig. 3. Bulk-rock SiO_2, FeO and MgO plotted against modal olivine (vol. %) in abyssal peridotites to show that the unexpected SiO_2–FeO–MgO systematics seen in Fig. 2 is controlled by mineral modes, particularly olivine modes, in these rocks. It should be noted that the relative standard deviations (% RSD) are significantly greater for mineral modes than for the constituent oxides (SiO_2, FeO and MgO).

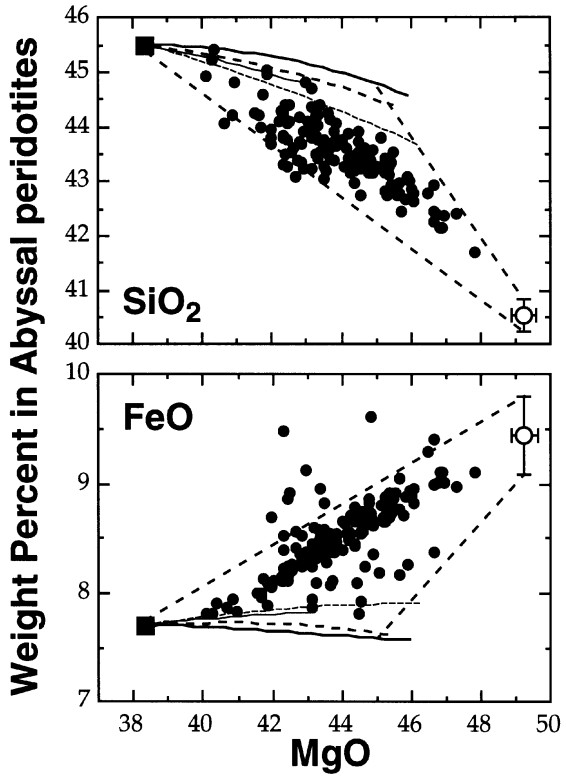

Fig. 4. MgO variation diagrams of SiO_2 and FeO for both data and model residues as in Fig. 2. Plotted also is the mean composition of olivine (○) in abyssal peridotites with 2σ variations. Clearly, the trends defined by most data points on the SiO_2–MgO and FeO–MgO plots are consistent with olivine addition. The fields enclosed by the dashed lines are where the mixtures of olivine and simple residues plot, with the simple residues being produced by varying degrees of melting from a single source composition (e.g. the preferred source, ■).

such a treatment neglects the role of *spinel*, which is not a serious problem because of the very low (<1·5%) *spinel* abundances in abyssal peridotites. Further simplifications are *opx* containing no Al component, and *cpx* containing no clinoenstatite and clinoferrosilite, which are certainly not true. However, as the purpose is to monitor how mineral proportions vary with melting, and to compare these variations that exist between abyssal peridotites and model melting residues, this simplification is justified as demonstrated in Fig. 5. The differences between norms and modes are systematic, and both norms and modes are related by the simple linear equations. That is, *ol*, *opx* and *cpx* modes can be readily obtained from their corresponding norms using the equations in Fig. 5.

Behaviour of Ol, Opx and Cpx during polybaric melting

Figure 6a shows how residual modes (scaled to a total mass of $1 - F$) produced by polybaric near-fractional melting vary with the extent of melting. Each line is a decompression melting path beginning at $P_o = 30$, 20 and 10 kbar, and ending at ~3 kbar. Figure 6a is best described by a reaction of the form

$$a\text{Cpx} + b\text{Opx} + d\text{Ol} + 1\text{melt} = 0. \qquad (1)$$

For a given melting path, a, b and d are corresponding slopes representing the melting modes (see Baker & Stolper, 1994), and are pressure (solidus depths) dependent. Their pressure dependence is even clearer in Fig. 6b, which also illustrates the following properties: (1) *ol* is the phase that is always being created ($d>0$),

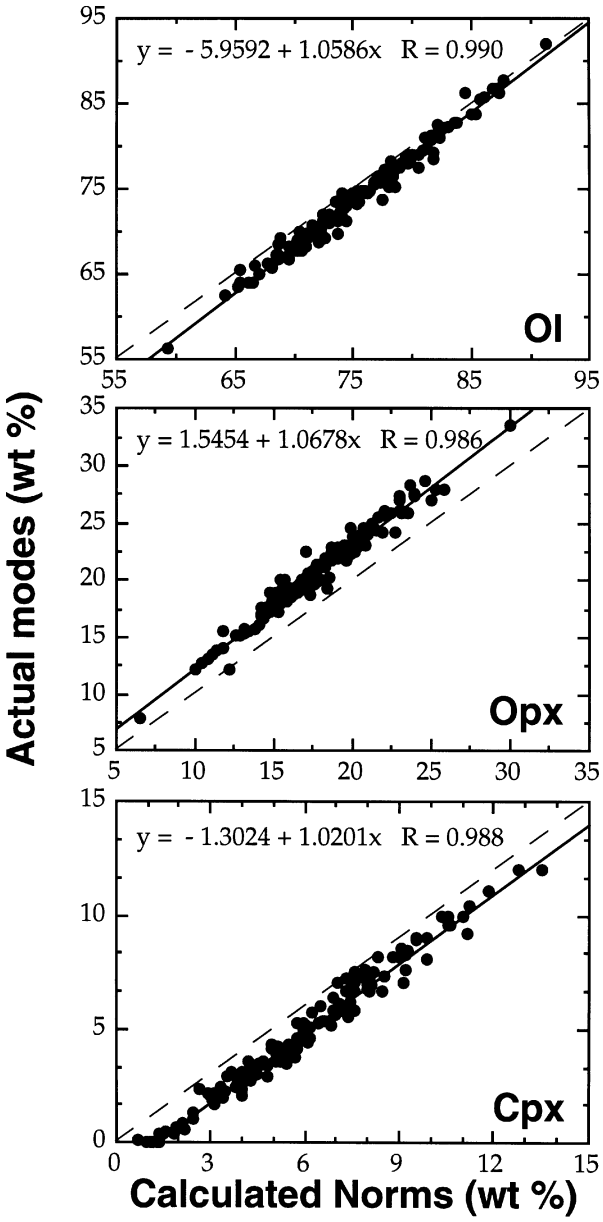

Fig. 5. The actual modes in abyssal peridotites (converted to wt %) plotted against the calculated norms from the constructed bulk-rock major element compositions using a procedure described in Appendix C. It should be noted that norms and modes are similar, and norms are readily converted to modes using the linear regression equations. The dashed lines are one-to-one reference lines.

whereas *cpx* (a<0) and *opx* (b<0) melt during decompression near-fractional melting at $P_o \leq 25$ kbar; (2) *cpx* melting mode is almost independent of pressure; (3) *ol* and *opx* melting modes are complementary; (4) *opx* contributes more than *cpx* to the melt (i.e. b is more negative than a).

The *opx–cpx* melting relationship (Fig. 6b), reported here for the first time, is an important property of polybaric melting, which has not been otherwise revealed through isobaric peridotite melting experiments without quantitative modelling. To fully explore the polybaric melting behaviour of major silicate mineral phases, equation (1) may be decomposed into three components:

$$\text{Cpx} \Rightarrow \text{melt}\ (F\uparrow, P\downarrow) \quad (2)$$

$$\text{Opx} \Rightarrow \text{melt}\ (F\uparrow, P\downarrow) \quad (3)$$

$$\text{Opx} \Rightarrow \text{Ol} + \text{SiO}_2\ (\text{in melt})\ (P\downarrow, F\uparrow) \quad (4)$$

in which $F\uparrow$ and $P\downarrow$ indicate qualitatively that melting proceeds with decompression. It should be noted that this decomposition is only meant to help understand equation (1) in terms of mass balance and some known properties of phase equilibria. A small capital P is used for equations (2) and (3) to indicate that decreasing pressure is equivalent to increasing temperature, allowing melting to occur (e.g. in the sense of isobaric conditions), which may have little effect on phase relations. In equation (4), decreasing pressure facilitates the reaction (see below).

These reactions indicate that in addition to continuous decompression melting of *cpx* and *opx*, an important effect of decreasing pressure is to convert Fe–Mg pyroxene (mainly *opx* plus clinoenstatite and clinoferrosilite) into *ol*, which crystallizes, while enriching SiO_2 in the melt. This results when *ol* phase volume (stability field) expands whereas *opx* phase volume (stability field) shrinks as pressure decreases (e.g. O'Hara, 1968*b*; Presnall *et al.*, 1979; Stolper, 1980). Figure 7 illustrates this well-characterized, yet poorly perceived, fact. Figure 7a is constructed from the well-known forsterite–enstatite–SiO_2 system originally studied by Bowen & Anderson (1914) at atmospheric pressure. The incongruent melting of enstatite to produce forsterite and liquid is the foundation of the liquid line of descent of Bowen (1928). It should be noted that enstatite would melt congruently at low pressures of a few kilobars in this highly simplified MgO–SiO_2 system (Boyd *et al.*, 1964; Chen & Presnall, 1975), but this does not occur in multicomponent systems that contain Al_2O_3 and involve *spinel* (Presnall *et al.*, 1979). Therefore, in multicomponent systems, as schematically illustrated in Fig. 7a, a peridotitic mantle that contains *ol* and *opx* will, upon melting, produce melts that lie at the reaction line (cotectic): Opx⇒Ol + SiO_2. The melt produced at a high pressure (P_1) will have low SiO_2 content (M_1), and the melt produced at a low pressure (P_3) will have high SiO_2 content (M_3), which is well known (e.g. Jaques & Green, 1980; Hirose & Kushiro, 1993). This reaction in multicomponent systems has been examined isobarically at 5 kbar (Kelemen *et al.*, 1990).

Beneath ocean ridges, decompression melting enhances this reaction because the reaction line (the cotectic) moves

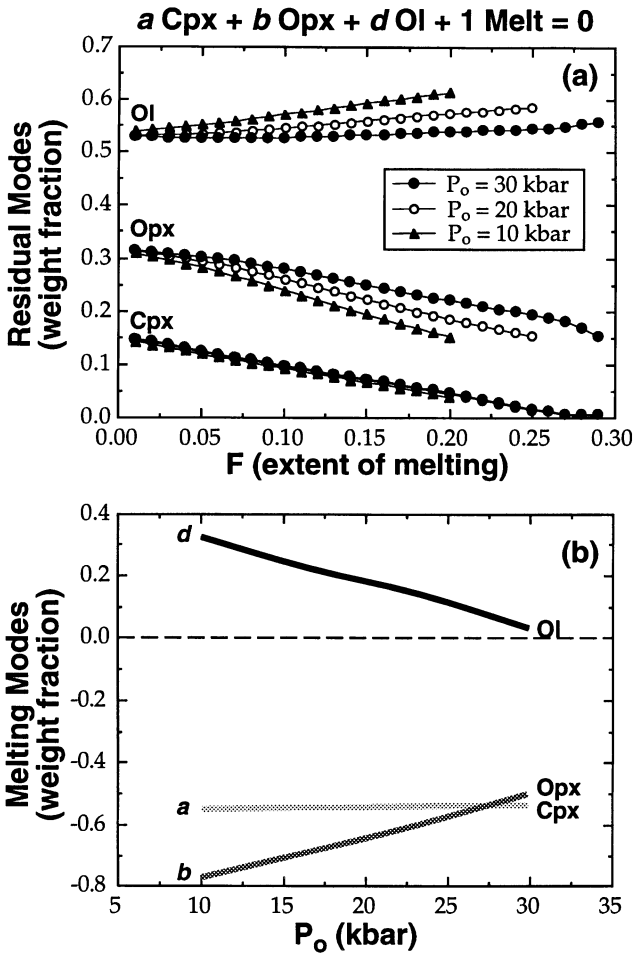

Fig. 6. (a) Residual *ol*, *opx* and *cpx* modes of polybaric near-fractional melting model (mNB91) residues plotted against the extent of melting (*F*). The modes are recast to a total mass of $1 - F$. Each line is a decompression path with increasing *F*, beginning at appropriate solidus depths (P_o = 30, 20, 10 kbar) and ending at ~3 kbar. Obviously, the slopes (melting modes) are strongly pressure dependent for both *ol* and *opx*, but not for *cpx*. (b) Melting modes, i.e. the slopes in (a), plotted against initial melting depth. Clearly, *ol* is being created, whereas *opx* and *cpx* melt during decompression melting. In the pressure range appropriate for MORB genesis *opx* melts more (is more negative) than *cpx*. It should be noted that the *opx*–*cpx* 'cross-over' is currently not well constrained because of limited experimental data in the 25–30 kbar pressure range.

towards the SiO_2-rich side as the melting mantle ascends. That is, pressure-release melting produces melt 'increments' progressively more SiO_2 rich by enhanced melting of *opx* and crystallization of *ol*, and gives a progressively higher *ol*/*opx* residue. This explains the complementary relationship between *ol* and *opx* melting modes with decreasing pressure (Fig. 6b). This simple concept is further illustrated in a more familiar ternary diagram 'projected' from *spinel* (Fig. 7b). The *ol* phase volume expands at the expense of *opx* phase volume whereas *cpx* phase volume is essentially constant. This schematic diagram differs from phase diagrams commonly used in that no SiO_2 is used as a component, and is in fact more informative because it reduces the number of components to the number of phases (*ol*, *opx*, *cpx* and *spinel*) that are physically present and involved in mantle melting, whereas SiO_2 is rather fictive.

As Fig. 6 uses low-pressure modes (converted from norms; see Fig. 5 and Appendix C) to reveal high-pressure signatures, the position of *cpx*–*opx* cross-over (Fig. 6b) may differ from that of actual polybaric melting residues without experiencing subsolidus equilibration (undetermined yet). Clearly, better controlled experiments in ~25–30 kbar range are needed. Also, *ol* will melt, and *opx* will crystallize at even higher melting pressures where *garnet* becomes the stable Al-rich phase (Walter & Presnall, 1994; Lesher & Baker, 1996). Nevertheless, the relative pressure-dependent melting relationships of *cpx* (*a*), *opx* (*b*), and *ol* (*d*) in Fig. 6 are considered valid (see below) at pressures appropriate for melting beneath ocean ridges.

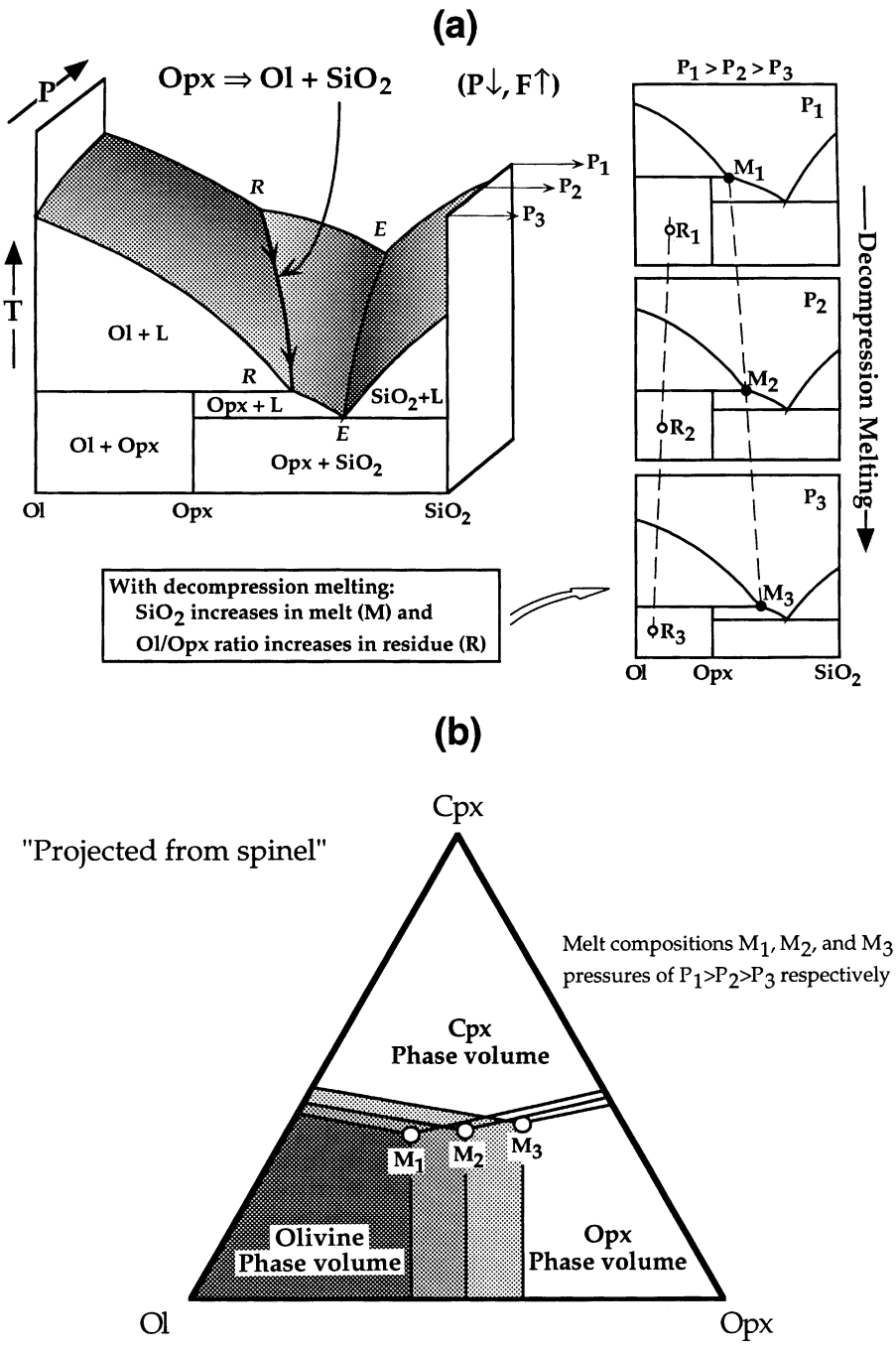

Fig. 7. (a) Schematic diagram of *ol–opx*–SiO_2 system, which is extended from the simple forsterite–enstatite–SiO_2 system, to show the reaction relationship between *ol* and *opx* described by equation (4) and illustrated in Fig. 6 as a function of pressure. (b) Qualitative illustration of a more familiar *ol–cpx–opx* ternary 'phase diagram' 'projected' from *spinel* to show the phase relations in Fig. 6. It should be noted that in this diagram, melts that are in equilibrium with the four phases (○) change towards SiO_2-rich (high normative *opx*/*ol*) compositions with decompression melting.

Geobarometry

Figure 6 and equation (1) also suggest that if the modes of a suite of residual peridotites are known, the initial melting pressure (P_o) and mean melting pressure (P_M) may be evaluated by the following empirical equations:

$$(0{\cdot}5536 - 0{\cdot}0008P_o)\mathrm{Cpx} + (0{\cdot}9100 - 0{\cdot}0135P_o)\ \mathrm{Opx} = (0{\cdot}4636 - 0{\cdot}0143P_o)\mathrm{Ol} + 1\mathrm{melt} \quad (5)$$

$$(0{\cdot}53815 - 0{\cdot}00065P_M)\mathrm{Cpx} + (0{\cdot}83746 - 0{\cdot}01683P_M)\mathrm{Opx} = (0{\cdot}37580 - 0{\cdot}01748P_M)\mathrm{Ol} + 1\mathrm{melt}. \quad (6)$$

These equations are polybaric expressions of equation (1), where the melting modes (i.e. *a*, *b* and *d*) in Fig. 6a are expressed as linear functions of initial (P_o) or mean (P_M) pressures (e.g. Fig. 6b). If *a*, *b* and *d* for a suite of residual peridotites are known, by equating these coefficients with the linear expressions in equations (5) and (6), P_o and P_M may be evaluated. Given the model uncertainties, and particularly, uncertainties in modal data of a given suite of residues, equation (6) is more meaningful for calculating mean melting pressure.

Applications

Derivation of the extent of melting from melting residues

Application of the above model results to a suite of residual peridotites requires the knowledge of *F*. This parameter can be estimated independently using whole-rock MgO contents in melting residues (Fig. 8), noting that the whole-rock MgO contents in residues produced by peridotite melting experiments vary linearly as a function of *F* (Fig. 8a). The scatter results from differences in starting compositions (e.g. different symbols) and melting pressures (e.g. as indicated by the lines of model residues of mNB91). TQLJG80 (MgO = 40·03 wt %) and KLBHK93 (MgO = 39·22 wt %) both are obviously too refractory relative to commonly suggested fertile mantle compositions (see Appendix B). If the starting compositions used in all these experiments are within the range of suggested upper-mantle compositions (e.g. the preferred source MgO = 38·3 ± 0·5% in Appendix B), the scatter largely disappears (Fig. 8b). The remaining, small, pressure effect on MgO is of the same order of magnitude as MgO uncertainties in both source composition and bulk-abyssal peridotites, and thus can be neglected for this purpose. Therefore, the linear relationship in Fig. 8c can be used to estimate the extent of melting from melting residues. It should be noted that using a single source MgO value that is within the suggested mantle compositional range is a necessary and reasonable assumption for modelling first-order problems on a large regional or global scale as attempted in this paper.

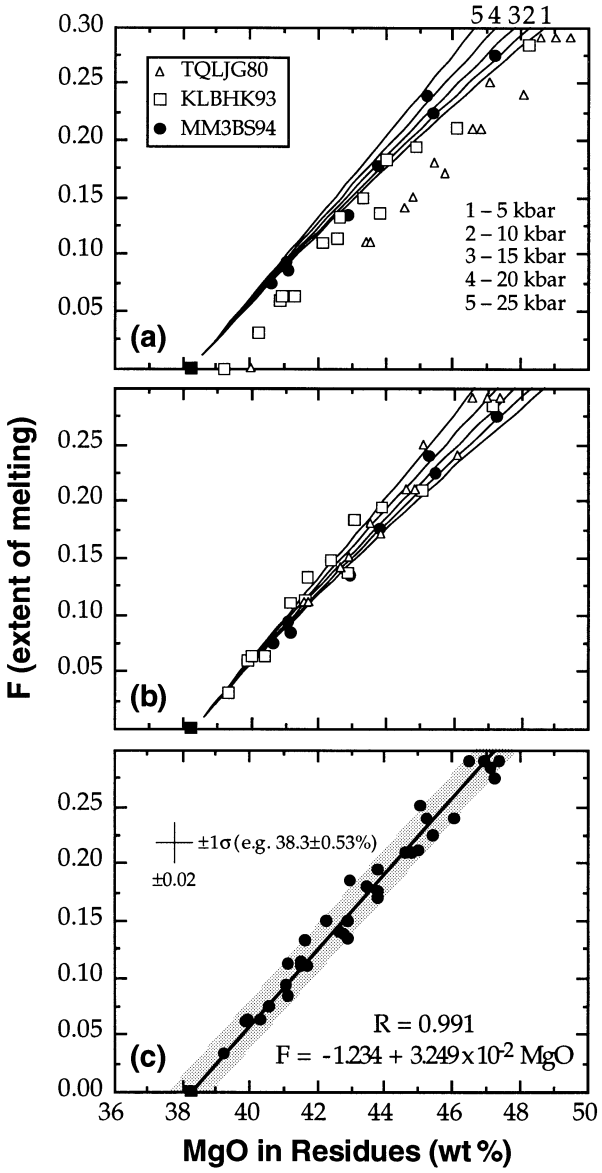

Fig. 8. Plots of the extent of melting vs MgO in experimental melting residues [TQLJG80 by Jaques & Green (1980); KLBHK93 by Hirose & Kushiro (1993); MM3BS94 by Baker & Stolper (1994)]. (a) The raw data; (b) the data after normalized to a common starting material (e.g. the preferred source: MgO = 38·3% in Appendix B); (c) the regression line used to estimate the extent of melting from bulk-rock MgO of residual peridotites. The shaded band in (c) indicates the 2σ variability of the calculated *F* values caused by the 2σ variability of MgO in the suggested mantle compositional range (see Appendix B). The *F* values for KLBHK93 were calculated using equation (5) for TQL of Niu & Batiza (1991*a*).

The *F* values calculated in such a way are plotted against modal *cpx* for several peridotite suites (Fig. 9). The large range (2σ) in the calculated *F* value for a given suite ultimately results from large modal variations within each suite (Dick, 1989). The inverse correlation between

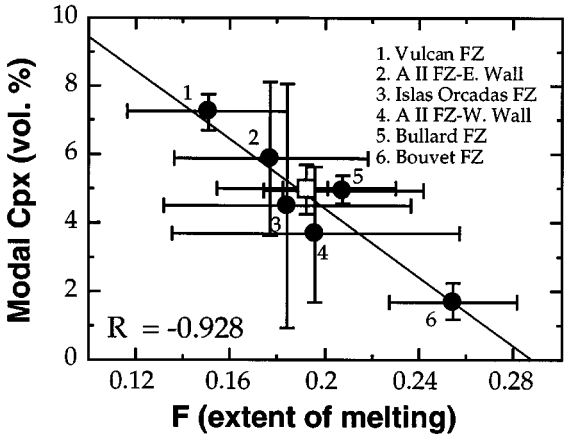

Fig. 9. Plot of the average modal *cpx* (vol. %) against the average extent of melting calculated from the bulk-rock MgO using the relationship in Fig. 8c for several abyssal peridotite suites (bars are 2σ). □, average of the entire data set.

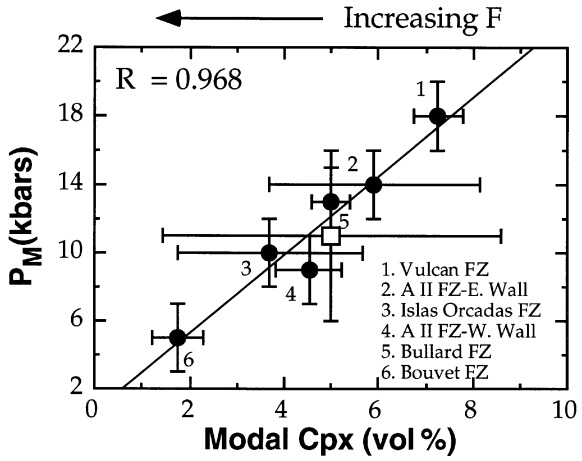

Fig. 10. Modal *cpx* (vol. %) plotted against the calculated melting pressures for several abyssal peridotite suites (as in Fig. 9). As modal *cpx* is inversely related to the extent of melting (*F*), this correlation thus indicates an inverse F–P_M, which is unexpected. (See text for discussion.)

the calculated F and modal *cpx* is consistent with the notion that the extent of mantle melting is high beneath ridges affected by a hotspot (e.g. Bouvet), and is low beneath ridges away from a hotspot (e.g. Vulcan). It should be noted that the calculated F values are rather high for all the suites, and for the entire data set as a whole (~19·2±3·8%).

An inverse P–F correlation—a problem

Applying equations (5) and (6) to the entire abyssal peridotite data set (see Appendix D for coefficients) gives $P_o = 19 \pm 5$ kbar and $P_M = 11 \pm 5$ kbar, which do not seem unreasonable. However, the results are unexpected for individual peridotite suites. For example, Fig. 10 shows that there is a positive correlation between the calculated mean melting pressures and average *cpx* modes in those abyssal peridotite suites shown in Fig. 9. As *cpx* modes inversely correlate with F (Fig. 9), Fig. 10 thus indicates an inverse P–F correlation, which is contrary to the notion that a hotter mantle (e.g. near Bouvet hotspot) begins to melt deeper and produces more melt than a colder mantle (e.g. near Vulcan) (e.g. Klein & Langmuir, 1987; McKenzie & Bickle, 1988; Niu & Batiza, 1991*a*). These calculations suggest that residual peridotites of high degrees of melting (e.g. near Bouvet hotspot) preserve signatures of more shallow level melt–solid equilibration than residual peridotites of low degrees of melting (e.g. Vulcan).

It is clear from Figs 6 and 7 that the calculated pressures are inversely related to *ol*/*opx* ratios in the solid residues. Thus, there are three scenarios that may help explain the inverse P–F correlation in Fig. 10:

(1) A mantle yields more melt by having a taller melting column with a shallower final depth of melting or melt segregation, leading to signatures of a lower equilibration pressure in residual peridotites. In this case, *ol* crystallization and *opx* melting follow the decompression melting reaction [equation (1); Fig. 6], producing normal residues with no olivine excess nor *opx* deficiency.

(2) Melts formed at depth will migrate upward and laterally towards the ridge axis. These melts may react actively with the ambient rock during ascent as proposed by Kelemen *et al.* (1995*a*, 1995*b*). This reaction is replacive, and creates excess olivine (dunites) while dissolving *opx* in the wall-rock at high melt/rock ratios. The consequence of this reaction is to produce excess olivine at the excessive loss of *opx* relative to residues produced by decompression melting [equation (1); Fig. 6], leading to higher *ol*/*opx* ratios in the residue, and hence lower calculated pressures.

(3) Ascending melts will crystallize *ol* when encountering the conductive thermal boundary layer at shallow levels, creating excess *ol* without dissolving *opx* in residual peridotites (Niu *et al.*, 1997; also see above). This will also lead to higher *ol*/*opx* ratios in the residue, and thus lower calculated pressures. We can test which of these scenarios is more plausible. As the melting mode of *cpx* is almost pressure independent, whereas those of *opx* and *ol* change significantly in a complementary manner during decompression melting (see Fig. 6), the test is thus simplified to examination of the differences between peridotites and model melting residues in terms of *ol* and *opx*, which involve primarily SiO_2, FeO and MgO.

Excess olivine or opx depletion or both?

Although a rigorous test requires accurate knowledge of the actual melting pressures, an estimate can be made

by comparing abyssal peridotites with the model melting residues (Figs 1 and 2). As the peridotites define trends on SiO_2–MgO and FeO–MgO diagrams that converge toward the fertile model source composition (Figs 2 and 4), the task is to rotate the data array relative to the source composition on the two diagrams to match model melting residues. The explicit assumptions are (1) polybaric near-fractional melting, and (2) initial melting pressures (P_o) lying in the range of 20–30 kbar. Thus, addition of SiO_2, subtraction of FeO, and required adjustment of MgO (stoichiometric considerations for both *ol* and *opx*) are equivalent to removing excess *ol* or adding *opx* that may have been 'dissolved', or both. Numerically, the algorithm is a simple mass balance equation:

$$\mathrm{Ox}^{\mathrm{AP}} = f^{\mathrm{Ol}}\mathrm{Ox}^{\mathrm{Ol}} + f^{\mathrm{opx}}\mathrm{Ox}^{\mathrm{opx}} + (1 - f^{\mathrm{Ol}} - f^{\mathrm{opx}})\mathrm{Ox}^{\mathrm{MR}} \quad (7)$$

where Ox refers to weight percent SiO_2, FeO and MgO; AP is the abyssal peridotite bulk compositions; MR represents the model melting residues (see Figs 1, 2 and 4); f^{Ol} and f^{opx} are weight fractions of the two phases in peridotites with appropriate compositions. We thus have three equations (three oxides) and three unknowns (f^{Ol} and f^{opx}, and *mg*-number of *ol* and *opx*, assumed the same for both). Although various Fo and En values were tried, Fo_{89} and En_{89} yield best fits to the entire data set (for all the samples), as shown in Fig. 11.

Fig. 11a plots all the data points and Fig. 11b plots averages for individual sample suites against the extent of melting. Obviously, abyssal peridotites differ from simple residues only by having excessive amounts of *ol* without gain or loss of *opx*. This is inconsistent with scenarios (1) and (2), but is consistent with scenario (3) that the inverse *F*–*P* correlation in Fig. 10 preserved in abyssal peridotites results from the ascent and cooling of mantle melts in the shallow thermal boundary layer near the surface. All the sample suites (Fig. 11b) have excess olivine, but the excess olivine increases with increasing *F* from Vulcan, distal to the hotspot, to Bouvet, near the hotspot, with a mean value of ~29 ± 11%. The positive correlation of the amount of excess olivine with *F* also is consistent with scenario (3) (Niu *et al.*, 1997; also see below). It should be noted that the extent of melting plotted is now recalculated (using fig. 8c) after excess olivine is removed (see Appendix E), and the mean extent of melting for the entire data set now is $F = 15{\cdot}4 \pm 5\%$ (vs $19{\cdot}2 \pm 3{\cdot}8\%$ before excess *ol* removal).

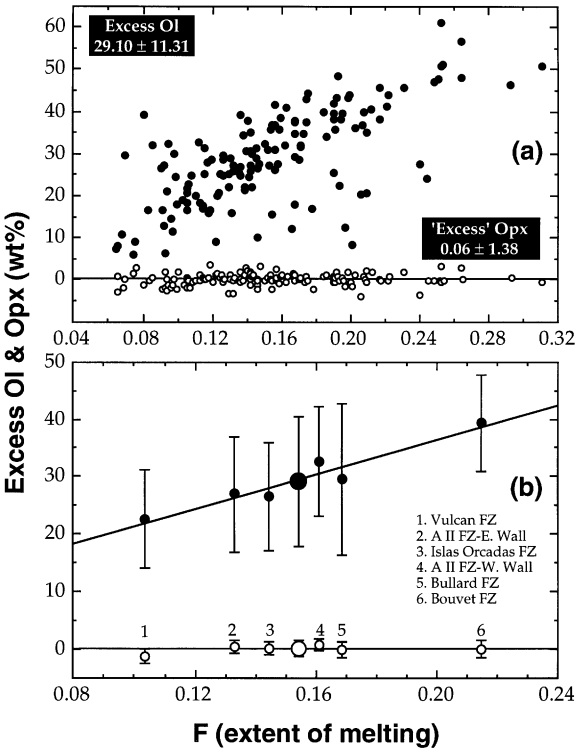

Fig. 11. Calculated excess *ol* and 'excess' *opx* plotted against the extent of melting (*F*, recalculated after excess olivine is removed) for all the data (a) and for suite averages (b). Clearly, the amount of excess olivine present in abyssal peridotites is proportional to the extent of melting or depletion these peridotites experienced. There is no *opx* excess or deficiency. The large circles in (b) are the mean values of the entire data set. The mean extent of melting now is $15{\cdot}6 \pm 5\%$ after excess olivine is removed (see Appendix E).

Melting reactions

Having removed the excess olivine that exists in abyssal peridotites, we can now examine the mineralogical systematics preserved in these residues. Figure 12 illustrates the residual *ol*, *opx*, *cpx* and *spinel* (recast to a total mass of 1 – *F*) plotted against *F*. The slopes of the regression lines, i.e. the melting modes, define a melting reaction:

$$a\mathrm{Cpx} + b\mathrm{Opx} + c\mathrm{Spl} = d\mathrm{Ol} + 1\mathrm{Melt} \quad (8)$$

where $a = 0{\cdot}466$, $b = 0{\cdot}652$, $c = 0{\cdot}049$ and $d = 0{\cdot}167$. This reaction is consistent with the decompression melting reaction [equation (1)] derived from mNB91 in that *opx* contributes more than *cpx* to the melt [i.e. *b*>*a*; see equations (1)–(4), and discussions]. This consistency reiterates the simple fact that mantle melting beneath ocean ridges results from decompression. Although uncertainties in these melting modes (coefficients) are difficult to evaluate because of combined uncertainties associated with modal data, the procedure of removing excess olivine [equation (7)], and pressure differences between different peridotite suites, the *cpx–opx–ol* melting relationship in equations (1) and (8) represent a new interpretation facilitating a better understanding of the decompression-induced polybaric melting process beneath ocean ridges.

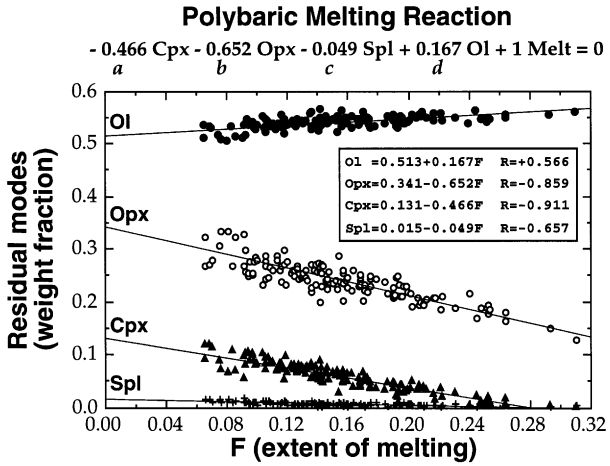

Fig. 12. Weight fractions of mineral phases (calculated to a total mass of $1 - F$) in residual abyssal peridotites (after removing excess *ol*) plotted against the extent of melting (F). The slopes of the regression lines, i.e. the melting modes of four phases, define a melting reaction similar to equation (1). This reaction indicates that to produce one mass unit of melt, 0·466*cpx*, 0·652*opx* and 0·049*spinel* must melt, and 0·167*ol* must be created. It should be noted that *opx* (0·652) contributes more than *cpx* (0·466) to the melt. This is consistent with equations (1)–(4) and Fig. 6, and reiterates that mantle melting beneath ridges is caused by decompression. The regression lines that give initial source modes (intercepts) and melting modes (slopes) are statistically significant at >99% levels. It should be noted that the *opx–cpx* melting relationship (i.e. $b>a$) is not an artefact of equation (7), as this relationship exists in abyssal peridotite raw data as well (Appendix D).

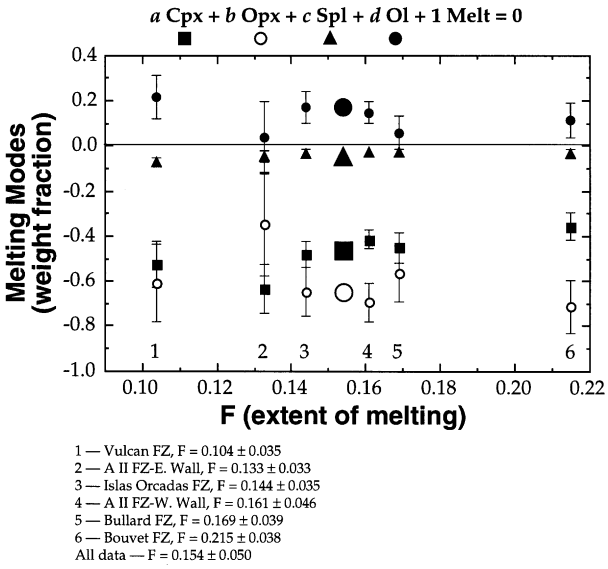

Fig. 13. Melting modes, determined as in Fig. 12, for individual abyssal peridotite suites plotted against the extent of melting. For comparison, the melting modes for the entire data set [i.e. coefficients for equation (8)] are also plotted using large symbols.

It should be noted that although decompression melting may begin at depths where *garnet* is a stable Al phase (e.g. Salters & Hart, 1989), the systematics in Figs 8 and 12 are consistent with the notion that partial melting beneath ocean ridges occurs primarily in the *spinel* lherzolite stability field (e.g. McKenzie & Bickle, 1988; Niu & Batiza, 1991*a*). If melting in the *garnet* lherzolite stability depth range were significant, we would see modal systematics in which *ol* decreases whereas *opx* increases with increasing extent of melting or depletion in residual peridotites (e.g. Walter & Presnall, 1994; Lesher & Baker, 1996), and abyssal peridotites would have higher SiO_2 and lower FeO as seen in cratonic lithosphere (Boyd, 1987, 1989; Cox *et al.*, 1987). These are not observed.

Additional calculations were done for individual peridotite suites (Fig. 13 and Appendix E). Obviously, equation (8) applies to the individual peridotite suites as well as the entire data set (large symbols): *ol* forms ($d>0$) whereas *opx*, *cpx* and *spinel* melt (a, b and $c<0$) during melting, except for the A II FZ E-Wall suite, which shows *cpx* melting more extensively than *opx*, although with large errors. These melting modes are based on fewer data points, and thus have larger uncertainties, relative to melting modes in equation (8) for the entire data set (the large symbols in Fig. 13).

DISCUSSION

Petrogenesis of abyssal peridotites

Mass balance calculations and phase equilibrium considerations presented above demonstrate that abyssal peridotites are not simple residues, but possess excess olivine. More excess olivine is present in residues of higher extents of melting (Fig. 11). This can be readily understood if we consider the thermal structure beneath a ridge in combination with some well-established igneous phase equilibria. Figure 14 illustrates that the mantle temperature profile beneath a ridge is determined by both convective (adiabat) and conductive thermal gradients. An adiabatic upwelling mantle begins to melt when intersecting the solidus at a depth P_o. Continuous melting is accompanied by continuous upwelling until the mantle reaches the near-surface thermal boundary layer at a shallow level P_f, which is determined by the conductive thermal gradient. In the melting region between P_o and P_f, decompression melting is characterized by the reaction aCpx + bOpx + cSpl = dOl + 1Melt [equation (8)]. This reaction produces *ol*, but is the polybaric melting process that generates true melting residues, and does not create excess olivine.

In the thermal boundary layer, melting stops, but melts produced over a wide region and depth range in the

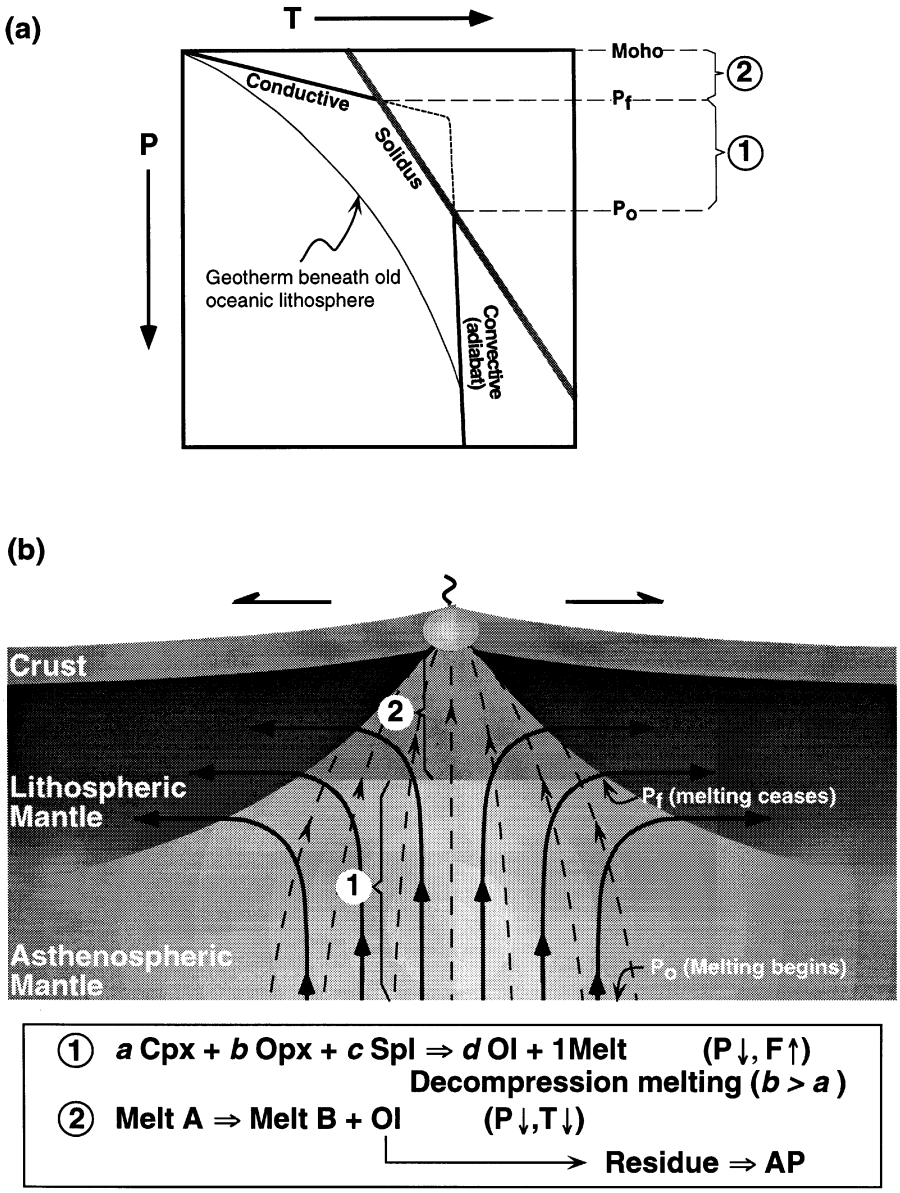

Fig. 14. (a) Diagram showing that the mantle beneath a ridge is conveniently considered as two regions: (1) the melting region between the solidus (P_o) and the final depth of melting (P_f) and (2) the conductive thermal boundary layer between P_f and the Moho. (b) Diagram showing that in (1), decompression melting is characterized by the polybaric melting reaction [equations (1) and (8)]; and in (2), ascending melts cool and crystallize olivine in the previously depleted residues. Bold lines with arrows are mantle flow lines; dashed lines with arrows are schematic paths of melt migration towards the ridge axis.

mantle must pass through this thermal boundary layer towards the ridge axis to form the crust. These melts cool and crystallize minerals that are on the liquidus. As olivine phase volume (stability field) expands with decreasing pressure (see Fig. 7; Niu *et al.*, 1997), olivine will be on the liquidus upon cooling at shallow levels. Hence, the combination of the physical condition and phase equilibria leads to olivine crystallization as an inevitable consequence of melt ascent and cooling beneath ocean ridges. Therefore, abyssal peridotites sampled at the surface are mixtures of melting residues and excess olivine formed in this way. That more olivine has been added to more depleted abyssal peridotites (Fig. 11) is also consistent with melting and melt transport process. Mantle melts vary in their normative olivine content, which is proportional to the extent and pressure

of melting (e.g. O'Hara, 1968*b*; Presnall *et al.*, 1979; Stolper, 1980; Jaques & Green, 1980) (also see Fig. 7). Thus, where melting begins deeper, the mantle melts to a greater extent, producing residues that are more depleted, larger melt volumes, and melt compositions that have higher normative olivine. Therefore, the most depleted residues are associated with olivine-rich melts. These melts will crystallize greater proportions of olivine as they enter the cooler thermal boundary layer at shallow levels.

Comparisons with other models

Melt refertilization model

Elthon (1992) concluded, based on reconstructed whole-rock compositions, that abyssal peridotites were too rich in Na_2O (on a Na_2O–MgO diagram) to be simple residues (e.g. the left panels of Fig. 15, and Fig. 2), but were consistent with refertilization by a compositionally variable melt component. Indeed, submersible observations (Cannat *et al.*, 1990; Hékinian *et al.*, 1992, 1993, 1995; Niu & Hékinian, 1997*b*) indicate that late-stage melt migration–percolation in residual peridotites can be locally pervasive. Niu & Hékinian (1997*b*) demonstrated that refertilization can be significant in modifying bulk-rock trace element compositions even in peridotites macroscopically unaffected by impregnation. However, the type of refertilization in whole-rock analyses observed by these workers may not be obvious in reconstructed bulk compositions. Figure 15 shows that TiO_2 and Na_2O contents are even higher after excess olivine is removed (right panels), yet can be reasonably well described by melting with the trends being closer to 'batch melting' curves. The key is that abyssal peridotites are not simple residues but possess excess olivine. Removal of excess olivine decreases bulk-rock MgO, but increases TiO_2 and Na_2O contents in the whole rock.

Melt–rock reaction model

Dunites are observed in mantle sections of many ophiolites (e.g. Dick, 1977*a*, 1997*b*; Nicolas, 1986, 1989; Kelemen & Dick, 1995). Kelemen *et al.* (1995*a*, 1995*b*) interpreted these dunites as resulting from melt–solid reactions (i.e. dissolution of pyroxene with concomitant precipitation of olivine) during melt ascent. This model and the model proposed in this paper both emphasize the effect of pressure on basalt melt phase equilibria, i.e. crystallization of *ol* and melting of *pyroxenes* in response to decompression. However, significant differences exist between the two models:

(1) The Kelemen *et al.* reaction model does not specify the depth range in which the melt–solid reaction takes place. The model proposed in this paper envisions the mantle beneath a ridge as two regions (see Fig. 14): the melting region in which melting is characterized by the decompression melting reaction [equation (8)], and a cold thermal boundary layer atop the mantle in which ascending melts crystallize *ol* as a result of cooling.

(2) The Kelemen *et al.* reaction model emphasizes the macroscopic observations, e.g. attempting to explain localized replacive dunites. The model proposed in this paper emphasizes the petrographic observations on residual peridotites (presumably away from these localized dunites), e.g. attempting to quantify the origin of excess *ol* and modal systematics in residual peridotites in the context of mantle melting and melt extraction processes beneath ocean ridges.

Therefore, the two models are complementary.

Other important implications

Primary magma issue

The composition of primary magma parental to MORB has been debated for ~30 years, with two extreme interpretations: (1) picritic liquids formed by 20–30% melting at pressures of ~20–30 kbar, and (2) tholeiitic liquids formed by 10–20% melting at shallower depths (~10 kbar) [see Elthon (1989) and Baker & Stolper (1994) for reviews]. The debate has been primarily based on interpretations of primitive MORB liquids using simplified phase diagrams constructed from isobaric experiments. Arguments from recent polybaric melting model calculations (e.g. Klein & Langmuir, 1987; McKenzie & Bickle, 1988; Niu & Batiza, 1991*a*) suggest that the definition of 'primary magma' needs revision, because MORBs are aggregates of liquids produced over a wide region and depth range of pressures. Polybaric melting models (Klein & Langmuir, 1987; Niu & Batiza, 1991*a*; Kinzler & Grove, 1992) predict that the primary melts parental to MORB would have MgO in the range of 11–14 wt %, yet hardly any primitive MORB melts observed fall in the range. Fractional crystallization in the crustal magma chambers surely will lead to more evolved compositions, which is particularly true along the fast-spreading East Pacific Rise, where steady-state magma chambers exist (e.g. Sinton & Detrick, 1992; Batiza *et al.*, 1996). The relatively less evolved nature of MORB melts from the Mid-Atlantic Ridge has been interpreted to result from lack of a crustal magma chamber, but the observed MgO values are still far lower than predicted for primary melts. The excess olivine observed in abyssal peridotites suggests that olivine crystallization at shallow mantle levels may be the primary cause of the evolved nature of MORB melts. Although the aggregated melts beneath a normal ocean ridge may not have MgO contents as high as proposed by O'Hara (1965, 1968*a*), he is certainly correct in deducing that all the MORB melts, even the most primitive ones, must have had lost a significant amount of olivine at shallow levels relative

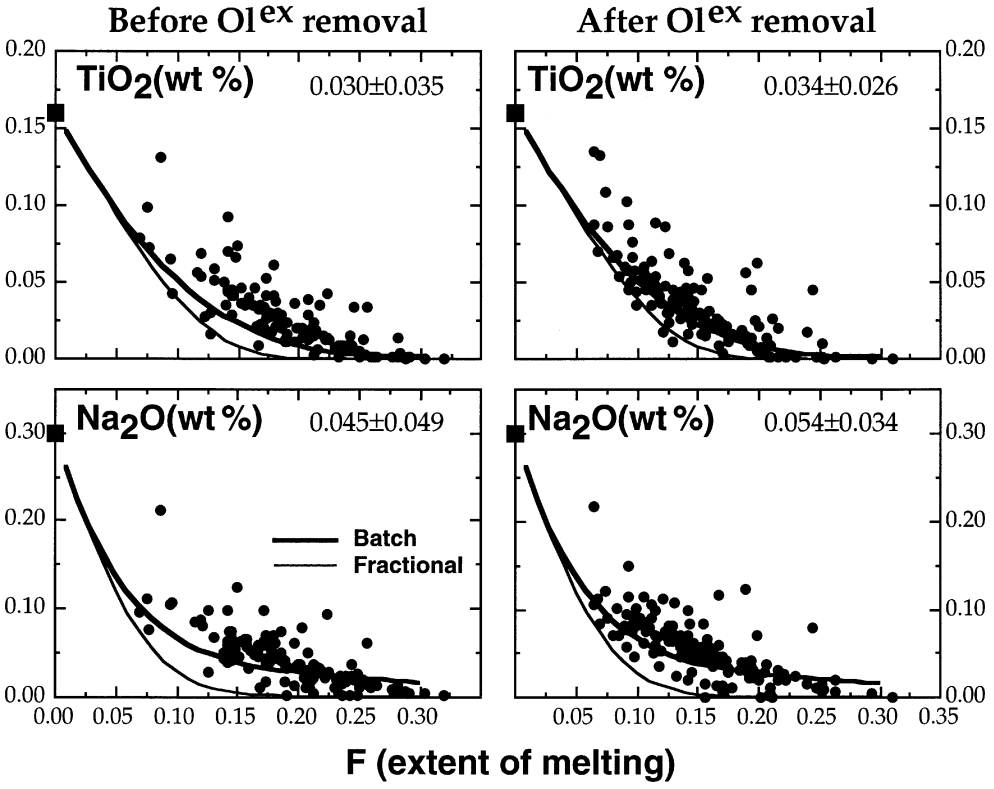

Fig. 15. Whole-rock TiO_2 and Na_2O plotted against the extent of melting calculated before (see Fig. 2) and after excess olivine is removed. Batch melting and near-fractional melting curves are plotted for comparison. Averages and 1σ values for TiO_2 and Na_2O are shown.

to their parent produced in the mantle (e.g. Walker *et al.*, 1979; Stolper, 1980). The implication is that neither the most primitive MORB melts nor bulk oceanic igneous crust is comparable with partial melts produced by peridotite melting experiments.

Final depth of melting (P_f)

Earlier models for MORB genesis assumed that pressure-release melting continues up to the Moho (e.g. Ahearn & Turcotte, 1979; Klein & Langmuir, 1987; McKenzie & Bickle, 1988). Niu & Batiza (1991*a*) showed that mantle melting beneath ocean ridges stops at levels significantly deeper than the Moho because MORB chemistry is inconsistent with melting to the Moho. Niu & Batiza (1991*a*, 1994) inferred that melting cessation may be caused primarily by increased heat of fusion of residual solid as a result of progressive depletion (e.g. compositionally more refractory). Asimow *et al.* (1995) argued that the effect of pressure-induced solid–solid phase transitions (i.e. *garnet–spinel* and *spinel–plagioclase* stability field transitions) is to suppress melting, and may potentially be the cause of melting cessation beneath ocean ridges. Shen & Forsyth (1995) emphasized the importance of conductive cooling in determining the final depth of melting. The observation that abyssal peridotites possess excess olivine whose origin is most consistent with crystallization from ascending and cooling melts provides direct evidence for the presence of a cold thermal boundary layer at mantle levels discussed in this paper (see Fig. 14; also see Niu *et al.*, 1997). In a recent case study of the basalt–peridotite association in the Garrett transform, Niu & Hékinian (1997*b*) showed that cooling and olivine crystallization of ascending melts in this thermal boundary layer can even lead to incompatible trace element enrichment in the whole-rock peridotites.

Importantly, Niu & Hékinian (1997*a*) showed that abyssal peridotites and MORB both consistently suggest that the extent of mantle melting beneath normal ocean ridges thermally unaffected by hotspots increases with increasing spreading rate. This observation, which is consistent with model predictions (e.g. Reid & Jackson, 1981), suggests that conductive cooling exerts the primary control on the final depth of melting. This is because fast spreading leads to fast upwelling, and fast upwelling beneath fast-spreading ridges allows the adiabat to extend to a shallower level against conductive cooling to the surface. Consequently, decompression melting continues up to a shallower level and more melt is produced from

a given parcel of mantle beneath fast-spreading ridges than beneath slow-spreading ridges. Decompression melting beneath ocean ridges does not, therefore, continue to the Moho, but rather stops in the mantle, whose depth is determined primarily by the conductive thermal gradient, which is spreading rate dependent (Niu & Hékinian, 1997*a*). Although a precise determination of the final depth of melting is unconstrained at present, and requires more observational data, there is the suggestion from S-wave seismic velocity data (Zhang & Tanimoto, 1993) that melting may stop at depths ≥ 30 km beneath very slow spreading ridges, but at depths perhaps significantly less than 30 km beneath fast-spreading ridges.

The concept and nature of the global trend

The inverse Na_8–Fe_8 correlation defined by regionally averaged global MORB data (Klein & Langmuir, 1987), called the global trend (Klein & Langmuir, 1989), has been interpreted to result from mantle temperature variation of up to ~250 K. A hotter mantle begins to melt deeper, has a taller melting column, and thus melts to a greater extent (high Fe_8 and low Na_8) than a colder mantle (low Fe_8 and high Na_8). In contrast, Shen & Forsyth (1995) argued, following Natland (1989) and Albarède (1992), that such a correlation results largely from fertile mantle compositional variation, plus variation in final depth of melting.

Whereas Klein & Langmuir (1987) used MORB data on a global scale, the so-called global trend or chemistry–depth correlation shown by these workers is defined by data mostly from the Mid-Atlantic Ridge and ridges from the Indian Ocean (see Brodholt & Batiza, 1989; Klein & Langmuir, 1989; Niu & Hékinian, 1997*a*), where variation in extent of mantle melting revealed by MORB and abyssal peridotites (Dick *et al.*, 1984; Michael & Bonatti, 1985; Klein & Langmuir, 1987) is associated with long-wavelength ridge depth variations because of the presence of on-ridge or near-ridge hotspots (e.g. Iceland and Azores, etc.). Although hotspots are hot and can affect ocean ridge thermal structures when migrating ridges are close to them (e.g. Schilling, 1991; Ribe, 1996; Ito *et al.*, 1996), they exist tectonically independently of ocean ridges. Relatively few ridges or ridge segments are thermally affected by hotspots on a global scale. Therefore, the so-called global (MORB) trend, or global chemistry–depth correlation, does not describe normal ocean ridges that are of purely plate tectonic spreading origin, but rather describes the thermal and compositional consequences of hotspot–ridge interactions on various scales at slow-spreading ridges. For example, exclusion of the few anomalous ridges affected by hotspots from ridge petrological data sets leads to a clear suggestion that spreading rate variation is the primary variable that determines the extent of mantle melting beneath ocean ridges and MORB chemistry (Niu & Hékinian, 1997*a*).

Origin of slow-spreading ridge local trend

Batiza *et al.* (1988) pointed out that a positive Fe_8–Na_8 correlation in MORB, opposite to the global trend, exists for some ridges. Klein & Langmuir (1989) called the positive Fe_8–Na_8 correlation the local trend, but this has since been shown to characterize slow-spreading ridges (Niu & Batiza, 1993). Different models have been proposed to explain the origin of the local trend, including intra-column melting (Klein & Langmuir, 1989), high-pressure fractionation (Kinzler & Grove, 1992, 1993), and solid–melt interaction in an upwelling and melting mantle (Niu & Batiza, 1993, 1994). The chemical trends of intra-column melting have been shown to differ from the local trend (e.g. Niu & Batiza, 1991*a*). Polybaric fractionation involving *ol–cpx–plag* at elevated pressures is a possible process, but will not produce the chemical systematics of the local trend (e.g. Niu & Batiza, 1993). To explain the local trend, Niu & Batiza (1993) considered all the major element oxides (SiO_2, TiO_2, Al_2O_3, FeO, MgO, CaO and Na_2O), not just Na_2O and FeO, because chemical systematics in the melt are governed by phase equilibria, regardless of whether the process is melting or fractionation. Changes in Na_2O and FeO in the melt cannot occur alone, but must be accompanied by changes of other components when a phase crystallizes or melts. Thus, any process that is invoked to explain the Na_8–Fe_8 relationship must also explain the relationships of Ca_8/Al_8–Si_8/Fe_8 and Na_8–Si_8/Fe_8 that exist in the MORB suites in which the local trend is well defined. With this simple consideration, Niu & Batiza (1993) examined the global MORB data, and found that the local trend can be described in terms of mass balance by the reaction

$$\text{Pyroxene} + \text{Melt A} \Rightarrow \text{Olivine} + \text{Melt B} \quad (P\downarrow \text{ and } F\uparrow) \qquad (9)$$

that is occurring in an upwelling and melting mantle, and is a net melting reaction (Mass B>Mass A). Niu & Batiza (1993, p. 7897) suggested that detailed modelling of residual peridotites can provide a rigorous test on whether equation (9) is the cause of the local trend. Indeed, equation (9) is actually a different expression of equations (1) and (8), because it also contains the three component reactions [equations (2), (3) and (4)], the only difference being that equation (9) explicitly involves a melt component that is in contact with the solid, i.e. a process that is near fractional melting (1–2% melt retention). This process explains Na_8–Fe_8, Ca_8/Al_8–Si_8/Fe_8 and Na_8–Si_8/Fe_8 relationships. Importantly, this process also explains the positive Ti_8–Ni_8 and negative Ca_8–Ni_8 correlations, characteristic of MORB suites at slow-spreading ridges (Niu & Batiza, 1994).

The local trend can therefore be explained if melts are tapped at different levels, as determined by the thermal structure in the mantle. For example, at 26°S Mid-Atlantic Ridge, cold edge effect near offsets may cause melting to stop at a great depth, and melts tapped at this deep level will have chemical signatures of low degree (high Na_8 and low Ca_8/Al_8) and high pressure (low Si_8/Fe_8) of melting, whereas in the segment centre removed from the offsets, mantle will ascend and continue melting up to a shallow level. Melts tapped at this shallow level will have chemical fingerprints of high degree (low Na_8 and high Ca_8/Al_8) and low pressure (high Si_8/Fe_8) of melting. This suggests that the pressure signatures preserved in the melts only reflect the final depth of melt–solid equilibration, not the initial solidus depth (Niu & Batiza, 1994). It should be noted that olivine crystallization in the near-surface thermal boundary layer discussed above may be invoked to explain the positive Na_8–Fe_8 relationship of the local trend, but it cannot explain the Ca_8/Al_8 systematics, because olivine crystallization does not affect this ratio.

Disequilibrium, or equilibrium, or perfect fractional melting?

The accepted view on the mode of partial melting beneath ocean ridges has evolved in the last decade from batch melting (high melt porosity) to perfect fractional melting (zero melt porosity). Disequilibrium melting also has been proposed (e.g. Prinzhofer & Allègre, 1985), and formulated (e.g. Qin, 1992; Iwamori, 1994) to explain the Th–Ra excess observed in MORB. The fact that primitive basalts (*mg*-number = 68–72) differ from mantle peridotites (*mg*-number = 89–91) indicates that solid–liquid equilibrium [e.g. olivine $K_d^{Fe-Mg} \approx 0{\cdot}3 \pm 0{\cdot}03$ (Roeder & Emslie, 1970)] is required during melting. Furthermore, the recent U–Th–Ra–Pa study (Lundstrom *et al.*, 1994) shows that equilibrium, not disequilibrium, is necessary at all depths of melt migration, to explain the excesses of Th, Ra and Pa when realistic K_d values for these elements are considered.

Perfect fractional melting is, in essence, an equilibrium melting, but conceptually it requires efficient melt removal from the residues upon melt formation such that there is no melt retained in the melting mantle. Perfect fractional melting has gained a particular popularity because of three independent studies: (1) interpretation of ^{230}Th excess in MORB (e.g. McKenzie, 1985*a*); (2) olivine–liquid rheology (Cooper & Kohlstedt, 1986; Riley & Kohlstedt, 1990); (3) interpretation of *cpx* Zr–Ti systematics in abyssal peridotites (Johnson *et al.*, 1990). However, various lines of evidence indicate that a minimum level of melt porosity in the melting mantle is necessary. For example, Lundstrom *et al.* (1994) showed that melt porosity is required to explain U–Th–Ra–Pa disequilibrium. Hirth & Kohlstedt (1995) showed that mantle permeability is significantly reduced (i.e. porosity increased up to 5%) when rheology of more realistic pyroxene–olivine–liquid, not olivine–liquid, is investigated. Also, Baker *et al.* (1995) showed that experimentally produced very low degree (~2%) melts are SiO_2 rich, implying that these melts have elevated viscosities that may not allow efficient melt segregation before melt porosity reaches a few percent. Johnson & Dick (1992) also noted the necessity for finite melt porosity when modelling abyssal peridotite trace element data from the Atlantis II fracture zone. Significantly, the systematics of TiO_2 and Na_2O in bulk-rock abyssal peridotites are better described by 'batch' melting than by perfect fractional melting (Fig. 15), suggesting that melt extraction may be inefficient or incomplete relative to that expected for fractional melting. Therefore, perfect fractional melting is unlikely.

Geometry of melting region, style of mantle upwelling, extent of melting, and crustal thickness

The geometry of the melting region beneath ocean ridges is unknown. A cross-ridge triangular shape (e.g. Ahearn & Turcotte, 1979; McKenzie & Bickle, 1988; Plank & Langmuir, 1992; Langmuir *et al.*, 1992; Forsyth, 1993) is a reasonable approximation for a passive upwelling mantle (2D). Although a component of active upwelling (3D) as a result of melting-induced buoyancy (i.e. presence of a melt phase and density reduction of residual mantle) may also be present, and may become progressively important with decreasing spreading rate (e.g. Scott & Stevenson, 1989; Parmentier & Phipps Morgan, 1990), truly active upwelling may only occur beneath ridges thermally affected by hotspots (e.g. Iceland). Thus, a triangular shape remains a reasonable description of the melting region beneath normal ridges. However, the upper bound of the melting region should not be the base of lithosphere, because of conductive cooling to the surface (Fig. 16; also see Fig. 14 and previous discussions).

The extent of melting, F, is the mass of the melt produced by decompression melting relative to the mass of the fertile mantle before melting, depending on mantle potential temperature (i.e. P_o, the initial depth of melting) and conductive thermal gradient (i.e. P_f, the final depth of melting) beneath a ridge (see Fig. 14). However, the extent of melting is not precisely known, and is often estimated petrologically using MORB chemical parameters, such as Na_8 (Klein & Langmuir, 1987) and Ca_8/Al_8 (Niu & Batiza, 1991*a*). These parameters are by no means always reliable, because variations of these elements in MORB melts may also reflect source variations (e.g. Natland, 1989; Albarède, 1992; Langmuir *et al.*, 1992; Niu & Batiza, 1994; Shen & Forsyth, 1995). Thus, averages over some geographical scales are necessary to allow meaningful regional comparisons.

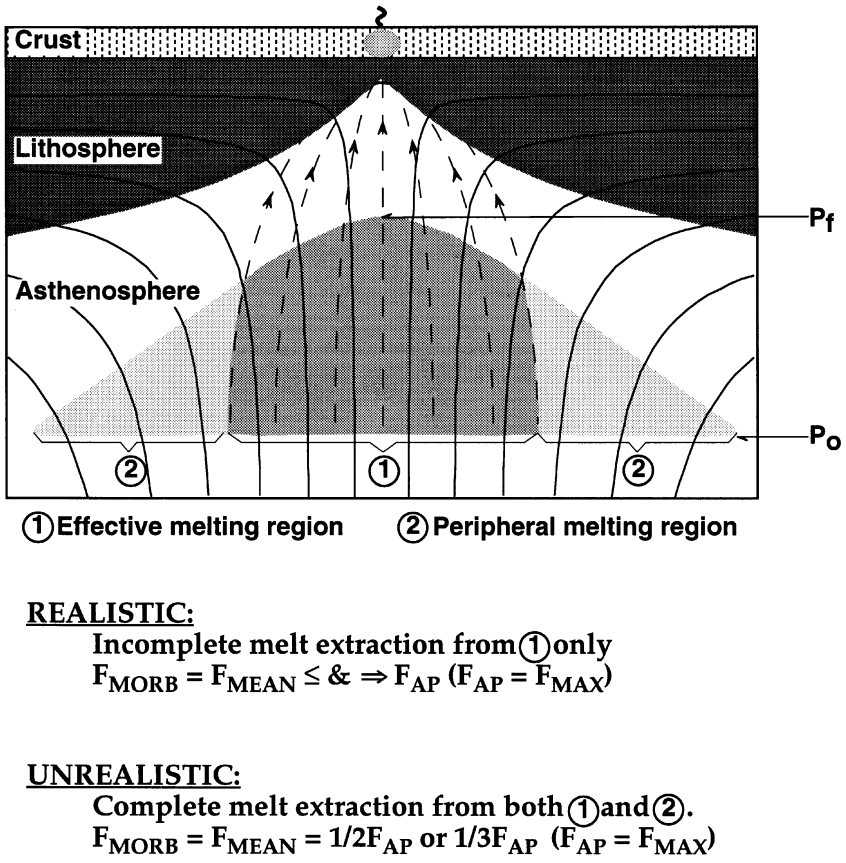

Fig. 16. Sketch showing that the geometry of mantle melting region in an across-ridge dimension may be approximated by a triangular shape with the upper bound determined by both vertical flow field and conductive cooling from the top. The extent of melting (F_{MORB}) derived by directly comparing MORB chemistry with model melts (e.g. Niu & Batiza, 1991*a*) is always equal to F_{Mean} relevant to crust formation because MORB melts are averages of extracted portions of mantle melts. $F_{Mean} = 1/2F_{Max}$ or $F_{Mean} = 1/3F_{Max}$ would be true only if melt extraction is complete, but cannot be true if melt extraction is incomplete. If only melts produced in the central, effective, melting region are extracted, F_{Mean} would be less than, but close to, F_{Max} indicated by abyssal peridotites (F_{AP}). Bold lines are mantle flow lines; dashed lines with arrows indicate melt migration paths.

The notion that oceanic crust thickness is more or less constant throughout ocean basins, and is independent of plate spreading rate (e.g. Chen, 1992; Bown & White, 1994) has been used as a constraint for models of MORB genesis (e.g. McKenzie & Bickle, 1988; Langmuir *et al.*, 1992; Forsyth, 1993; Kinzler & Grove, 1993). Crustal thickness is, however, entirely estimated using seismic velocity data, and may not be always reliable. For example, in the axial zones of some slow-spreading ridges where normal crustal thickness is suggested by seismic data, mantle peridotites dominate the crustal level, and igneous crust is essentially absent (Cannat, 1996). In addition, using *in situ* drill-hole data, Detrick *et al.* (1994) demonstrated that seismic layer 2/3 boundary in oceanic crust lies within sheeted dykes, and is determined by changes in crustal porosity and alteration, not by lithological changes from sheeted dykes to gabbros as widely thought. Therefore, seismic data must be used with caution (Cannat, 1996; Niu & Hékinian, 1997*a*) when interpreting the thickness and structure of oceanic crust.

In addition to the above difficulties, there is also a current debate as to how to estimate the extent of melting from petrological data. By considering the geometry of the melting region, Plank & Langmuir (1992) and Langmuir *et al.* (1992) introduced the concept of the mean (F_{Mean}) and maximum (F_{Max}) extent of melting. F_{Max} would be reflected in abyssal peridotites, which are likely to be the residues of maximum extent of melting in the central column that ascends to the highest level beneath a ridge (e.g. Dick *et al.*, 1984). F_{Mean} would be $1/2F_{Max}$ (Plank & Langmuir, 1992; Langmuir *et al.*, 1992) or $1/3F_{Max}$ (Forsyth, 1993), depending on definitions and model assumptions (Plank *et al.*, 1995). This treatment is theoretically correct only if melt extraction is complete, because MORB melts sampled at the surface would

represent mixtures of a range of low- to high-degree melts extracted from throughout the melting region (Fig. 16). However, the F_{Mean} values so calculated are misleading if melt extraction is incomplete. For example, melts produced in 'peripheral' regions (Fig. 16) may never come to the ridge axis, and do not contribute to crust formation at the axis. Complete melt extraction from mantle is unlikely, as is indicated by active near-ridge seamounts (Batiza *et al.*, 1990; Niu & Batiza, 1991*a*; Niu *et al.*, 1996) and implied by fluid dynamics models (e.g. Cordery & Phipps Morgan, 1993; Chen, 1996).

Niu & Batiza (1991*a*) estimated F by directly comparing the observed MORB melts with model melts. As MORB melts represent the pooled, net product of the extracted portion of the mantle melt, the mean extent of melting so derived therefore equates with F_{Mean}, which is pertinent to crust formation, and is less than, but approximates F_{Max} (Fig. 16; Langmuir *et al.*, 1992; Niu *et al.*, 1996). Using this approach, Niu & Batiza (1991*a*) concluded that MORBs represent extents of mantle melting between 10 and 21% with an average of ~16% on a global scale (see their fig. 13). This estimate is similar to $15 \pm 5\%$ independently determined from the abyssal peridotite data (Figs 11 and 13) in this study. Using the same approach, Niu & Hékinian (1997*a*) obtained average extents of mantle melting between ~10% at very slow spreading rates and ~22% at fast spreading rates on a global scale, comparable with the data obtained from abyssal peridotites (Niu & Hékinian, 1997*a*). These estimates of extent of melting are significantly higher than the value of $\leq 10\%$ that has been advocated to be the average global extent of mantle melting beneath ocean ridges (Klein *et al.*, 1991; Forsyth, 1993).

The higher (10–22%), not lower ($\leq 10\%$), extent of melting beneath ocean ridges is further constrained by two independent considerations. One is the observation that Ti is more incompatible than Na in many MORB suites (Niu & Batiza, 1994; Niu *et al.*, 1996), which requires $F_{Mean} \geq 15\%$; Na would be more incompatible than Ti if $F_{Mean} <$ ~15% (Niu & Batiza, 1994; Niu *et al.*, 1996). Another consideration is a simple mass conservation calculation. In a perfect passive upwelling mantle, the width of upwelling mantle is related to plate spreading rate as worked out by Reid & Jackson (1981): $U = 2Vz^2/[\pi(x^2 + z^2)]$, where U is mantle upwelling rate, V is half spreading rate, z is depth and x is distance away from ridge axis. $U_{Max} = 2V/\pi$ (when $x = 0$ right beneath the axis), and $U \leq 2V/\pi$ (in general). For simplicity, we let $U = U_{Max}$ everywhere across the ridge. As the mass of the crust produced per unit time must equal the mass of the melt produced on the same time scales in the mantle with complete melt extraction, then $2Vh = 2wUF$ must be true (the effect of density differences, ~10%, may be neglected for this purpose), where h is crustal thickness, w is half-width of upwelling–melting zone (i.e. one side of ridge axis) and F is the extent of melting of the mantle that enters the melting region. For a crust of, say, 6 km thickness, $w \geq 3\pi/F$ or $w \geq 9/F$.

This simple calculation [also see Phipps Morgan (1987)] indicates that for a perfect passive upwelling mantle, melt produced in the mantle as far as 180, 90, 60 and 45 km distance from both sides of the ridge must transport laterally towards the axis to form the 6 km crust if $F_{Mean} = 5\%$, 10%, 15% and 20%, respectively. These distances are the minimum values because upwelling rate, and hence melt production rate, decreases away from the axis. By accepting $F_{Mean} = 10\%$ (e.g. Klein *et al.*, 1991; Forsyth, 1993), one needs a mechanism to transport melt over distances of >90 km towards the ridge axis. In fact, it has been the focus of much recent research among theoretical modellers to search for mechanisms of melt transport towards the ridge axes over long distances of melt migration [see Turcotte & Phipps Morgan (1992)]. Cordery & Phipps Morgan (1993) showed that long-distance melt transport is difficult by two-phase flows without invoking a boundary layer channelling (beneath cold lithosphere lid) (Sparks & Parmentier, 1991). However, if one accepts F_{Mean} ~20%, rather than 10%, as proposed in this study and other studies (Niu *et al.*, 1996; Niu & Hékinian, 1997*a*, 1997*b*), melt produced within ~35 km on both sides of the ridge would be sufficient for a 6 km crust (Niu *et al.*, 1996), and there is no need to invoke long-distance (>70 km) lateral melt migration to ridge axes.

Melt migration, melt–rock reactions and pressure signatures in MORB melts

Melt formed at depth will ascend because of buoyancy (e.g. Ahearn & Turcotte, 1979; Stolper *et al.*, 1981). Melt segregation caused by matrix compaction (McKenzie, 1984) occurs as soon as the initial porosity exceeds the permeability threshold. The perceived permeability threshold has reduced significantly from up to 10% (e.g. Maaløe, 1982), to ~3% (McKenzie, 1984), and to several orders of magnitude less than 1% (McKenzie, 1985*a*, 1985*b*; Spiegelman & Elliot, 1993), to explain the observed Th–Ra excess in MORB. Recently, Hirth & Kohlstedt (1995) showed that an abrupt change in rheological behaviour of partially molten aggregates occurs at 5% (when wetting is achieved between two phase boundaries), and below this value the influence of melt on strain rate is rather modest. This suggests that compaction may be ineffective in inducing melt segregation in early stages of melting near the solidus. Melt migration may occur as diffusive porous flow or network-like channelling on millimetre scales (e.g. McKenzie, 1984; Turcotte & Phipps Morgan, 1992). Coalescence of these melts may allow development of 'veins' (e.g. Nicolas, 1986) or hydraulic 'cracks' (e.g. Sleep, 1988; Stevenson, 1989) for effective melt transport.

Whether these commonly held scenarios precisely describe the actual physics of melt segregation and transport is unconstrained at present. A common interpretation is that MORB melts retain geochemical signatures inherited at depth (Klein & Langmuir, 1987; Salters & Hart, 1989; Beattie, 1993; Bourdon *et al.*, 1996), which requires that melts formed at depths in the mantle be extracted rapidly without experiencing low-pressure equilibration during ascent (Langmuir *et al.*, 1992). Flows through large channels (Spiegelman & Kenyon, 1992) would help avoid low-pressure equilibration, but dyke-like large channels may only develop at much shallower depths where brittle deformation becomes important (e.g. Turcotte & Phipps Morgan, 1992; Dick & Natland, 1996). Recently, Kelemen *et al.* (1995*a*, 1995*b*) proposed that replacive dunite bodies in mantle sections of many ophiolites are reaction products of ascending melts with ambient mantle by dissolving pyroxenes. These dunites are thought to be conduits for subsequent melt transport, preventing chemical exchange between migrating melts and mantle rock at shallow levels. These workers provide evidence for the origin of replacive dunites, but these dunites may not be effective chemical 'insulators'.

The melt–rock reaction itself is an equilibration process as a result of melt decompression, which tends to eradicate signatures in the melt inherited at depth (e.g. increasing Si/Fe ratio, and leading to related trace element adjustments in the melt). Replacive dunites may, in fact, not be the major passages for melt transport because abyssal peridotites are not necessarily associated with replacive dunites (e.g. Niu & Hékinian, 1997*b*; Niu *et al.*, 1997). The observation that abyssal peridotites preserve polybaric melting reaction requires melting to be a process of continuous solid–liquid interaction, such that the melt would preserve pressure signatures of the final depth of solid–liquid equilibration. Importantly, all these peridotites possess excess olivine on thin-section scales, and the origin of the excess olivine is most consistent with the ascent and cooling of mantle melts in the near-surface thermal boundary layer. Niu & Hékinian (1997*b*) further demonstrated that the olivine crystallization is associated with whole-rock incompatible element refertilization. All these observations support porous flow as the dominant mode of melt migration, even at very shallow levels.

Recognizing that (1) porous flow is the primary means of melt transport, (2) the time scale for melt transport from melting region to the crust is of the order of thousands of years (e.g. McKenzie, 1984, 1985*a*, 1985*b*; Spiegelman & McKenzie, 1987; Rubin & Macdougall, 1988, 1990), and (3) no more than a few tens of hours are sufficient for attaining solid–melt equilibrium in peridotite melting experiments requires that low-pressure melt–solid equilibration is inevitable during melt ascent. Although geochemical 'depth' signatures may not be entirely erased during melt ascent because low-pressure equilibration is not the exact reverse of partial melting, these signatures in MORB melts, if preserved, may not be unequivocally revealed because of mantle source heterogeneity. For example, melting of a low-degree melt metasomatized mantle (Hirschmann & Stolper, 1996) or a mantle containing components of recycled oceanic crust (i.e. eclogite) (Niu & Batiza, 1997) at the *spinel* lherzolite depth may produce melts that have '*garnet*' signatures. Presence of eclogitic domains in a melting lherzolite mantle will affect not only major elements but also trace elements and even the amount of $^{230}Th/^{232}Th$ excess in partial melts (Lundstrom *et al.*, 1995).

Another example concerns how to explain the positive $[Sm/Yb]_N$–Na_8 correlation defined by regionally averaged MORB data from normal ridges (Shen & Forsyth, 1995). This correlation seemingly implies that deep melts [high $(Sm/Yb)_N$; more garnet signature] are associated with low degrees of melting (high Na_8), whereas shallow melts [low $(Sm/Yb)_N$; less garnet signature] are associated with high degrees of melting (low Na_8). Shen & Forsyth (1995) interpreted this correlation to result from varying final depths of melting; Langmuir (1995) interpreted it to be the result of the combination of low-degree melt effects and mantle temperature variation, whereas Salters (1996) interpreted it as being due to varying shapes of melting region. This correlation could, however, simply reflect the previous history of the fertile mantle, i.e. various extents of previous melt depletion/enrichment. Can we disapprove the statement, 'what we see in the melt largely reflects what is present in the mantle source'?

SUMMARY

(1) Abyssal peridotites are not simple residues, but mixtures of melting residues and excess olivine. The origin of this excess olivine is most consistent with the ascent and cooling of mantle melts. Melts produced over a wide region and depth range will ascend because of buoyancy and move laterally towards the ridge axis. These melts will crystallize olivine when passing through the previously depleted residues in the near-surface thermal boundary layer atop the mantle. The more melt that forms at depth, the more melt that passes through these residues, and the greater the amount of olivine that crystallizes in these residues.

(2) Decompression melting beneath mid-ocean ridges is characterized by the reaction aCpx + bOpx + cSpl = dOl + 1·000Melt, i.e. *cpx*, *opx* and *spinel* melt whereas olivine crystallizes as melting proceeds. In much of the pressure range ($P_o \leq 25$ kbar), *opx* contributes more than *cpx* to the melt (i.e. $b>a$), which is unexpected from isobaric experiments, but is consistent with melting models, and is constrained by the incongruent melting of Opx⇒Ol + SiO_2 with decreasing pressure. This melting reaction

also explains the so-called local trend of MORB chemistry characteristic of slow-spreading ridges (Niu & Batiza, 1993, 1994). This melting reaction provides so far the most realistic melting modes for trace element modelling.

(3) MORBs constitute no more than a few percent of the total oceanic crustal mass, and are not primary mantle derivatives. The bulk igneous crust is not comparable with partial melts produced in peridotite melting experiments because of olivine crystallization in the mantle. Therefore, MORB melts are not expected to be in equilibrium with mantle minerals in terms of both major and trace elements at any pressures.

(4) Porous flow is the primary mode of melt migration even at very shallow levels because excess olivine is observed on thin-section scales in all the abyssal peridotites thus far examined in detail (Niu & Hékinian, 1997*b*; Niu *et al.*, 1997).

(5) Low-pressure melt equilibration during ascent is unavoidable because the melting reaction preserved in residual peridotites requires continuous solid–liquid equilibration, and because olivine crystallization in the thermal boundary layer is the natural consequence of melt ascent and cooling; caution is necessary when inferring melting depths from basalt chemistry.

(6) Perfect fractional melting is unlikely. Significant (a few percent?) melt porosity in the melting mantle is required by (a) the melting reaction preserved in residual peridotites, (b) bulk-rock major element data, (c) solid–melt rheology behaviour (Hirth & Kohlstedt, 1995), (d) elevated viscosities of very low degree melts (very SiO_2 rich) near the solidus (Baker *et al.*, 1995), which may not allow efficient melt segregation, and (e) U–Th–Ra–Pa disequilibrium (Lundstrom *et al.*, 1994, 1995).

(7) As MORB melts are compositionally the averages of the extracted portion of the mantle melt relevant to crust formation, the extent of melting derived by comparing MORB melts with model melts (e.g. Niu & Batiza, 1991*a*) thus represents the mean extent of melting, F_{Mean}, which is less than but close to F_{Max} indicated by abyssal peridotites. Compositional variations of both MORB and abyssal peridotites are consistent with ~10–22% mantle melting beneath global ocean ridges.

ACKNOWLEDGEMENT

I appreciate useful discussions with Charlie Langmuir on many aspects of mantle melting processes, although we sometimes disagree. Discussions with Rodey Batiza, Henry Dick, Tony Ewart, Trevor Falloon, Dave Green, Peter Kelemen, Ro Kinzler and Shen-su Sun are very helpful. I particularly thank Charlie Langmuir, Rodey Batiza, Tony Ewart and Trevor Falloon for critical comments on an early version of the paper, which helped clarify some discussions. Thorough and critical reviews by Mike Bickle, Keith Cox, Don Elthon and Mike O'Hara were very helpful, and are acknowledged with great gratitude. Editorial effort by Tony Ewart is gratefully appreciated.

REFERENCES

Ahearn, J. L. & Turcotte, D. L., 1979. Magma migration beneath an ocean ridge. *Earth and Planetary Science Letters* **45,** 115–122.

Albarède, F., 1992. How deep do common basaltic magmas form and differentiate? *Journal of Geophysical Research* **97,** 10997–11009.

Asimow, P. D., Hirschmann, M. M., Ghiorso, M. S., O'Hara, M. J. & Stolper, E., 1995. The effect of pressure-induced solid–solid phase transitions on decompression melting of the mantle. *Geochimica et Cosmochimica Acta* **59,** 4489–4506.

Baker, M. B. & Stolper, E. M., 1994. Determining the composition of high-pressure mantle melts using diamond aggregates. *Geochimica et Cosmochimica Acta* **58,** 2811–2827.

Baker, M. B., Hirschmann, M. M., Ghiorso, M. S. & Stolper, E. M., 1995. Compositions of near-solidus peridotite melts from experiments and thermodynamic calculations. *Nature* **375,** 308–311.

Batiza, R., Melson, W. G. & O'Hearn, T., 1988. Simple magma supply geometry inferred beneath a segment of the Mid-Atlantic Ridge. *Nature* **335,** 428–431.

Batiza, R., Niu, Y. & Zayac, W. C., 1990. Chemistry of seamounts near the East-Pacific Rise: implications for the geometry of subaxial mantle flow. *Geology* **18,** 1122–1125.

Batiza, R., Niu, Y., Karsten, J. L., Boger, W., Potts, E., Norby, L. & Butler, R., 1996. Steady and non-steady state magma chambers below the East Pacific Rise. *Geophysical Research Letters* **23,** 221–224.

Beattie, P., 1993. Uranium–thorium disequilibria and partitioning on melting of garnet peridotite. *Nature* **363,** 63–65.

Bickle, M. J., 1986. Implications of melting for stabilization of the lithosphere and heat loss in the Archaean. *Earth and Planetary Science Letters* **80,** 314–324.

Bottinga, Y. & Allègre, C. J., 1973. Thermal effects of seafloor spreading and the nature of the oceanic crust. *Tectonophysics* **18,** 1–17.

Bottinga, Y. & Allègre, C. J., 1978. Partial melting under spreading ridges. *Philosophical Transactions of the Royal Society of London, Series A* **288,** 501–525.

Bourdon, B., Langmuir, C. H. & Zindler, A., 1996. Ridge–hotspot interaction along the Mid-Atlantic Ridge between 37°30′ and 40°30′N: the U–Th disequilibrium evidence. *Earth and Planetary Science Letters* **142,** 175–189.

Bowen, N. L., 1928. *The Evolution of the Igneous Rocks*. Princeton, NJ: Princeton University Press, 332 pp.

Bowen, N. L. & Anderson, O., 1914. The binary system MgO–SiO_2. *American Journal of Science, 4th Series* **37,** 487–500.

Bown, J. W. & White, R. S., 1994. Variation with spreading rate of oceanic crustal thickness and geochemistry. *Earth and Planetary Science Letters* **121,** 435–449.

Boyd, F. R., 1987. High- and low-temperature garnet peridotite xenoliths and their possible relation to the lithosphere–asthenosphere boundary beneath southern Africa. In: Nixon, P. H. (ed.) *Mantle Xenoliths*. New York: John Wiley, pp. 403–412.

Boyd, F. R., 1989. Compositional distinction between oceanic and cratonic lithosphere. *Earth and Planetary Science Letters* **96,** 15–26.

Boyd, F. R., England, J. L. & Davis, B. T. C., 1964. Effects of pressure on the melting and polymorphism of enstatite, $MgSiO_3$. *Journal of Geophysical Research* **69,** 2101–2109.

Brodholt, J. P. & Batiza, R., 1989. Global systematics of unaveraged mid-ocean ridge basalt compositions: Comments on 'Global correlations of ocean ridge basalt chemistry with axial depth and crustal thickness by Klein, E. M. and Langmuir, C. H.' *Journal of Geophysical Research* **94,** 4231–4239.

Cannat, M., 1996. How thick is the magmatic crust at slow-spreading oceanic ridges? *Journal of Geophysical Research* **101,** 2847–2857.

Cannat, M., Bideau, D. & Hébert, R., 1990. Plastic deformation and magmatic impregnation in serpentinized ultramafic rocks from the Garrett transform fault (East Pacific Rise). *Earth and Planetary Science Letters* **101,** 216–232.

Carmichael, I. S. E., Turner, F. J. & Verhoogen, J., 1974. *Igneous Petrology*. New York: McGraw–Hill.

Chen, Y. J., 1992. Oceanic crustal thickness versus spreading rate. *Geophysical Research Letters* **19,** 753–756.

Chen, Y. J., 1996. Constraints on the melt production rate beneath the mid-ocean ridges based on passive flow models. *Pure and Applied Geophysics* **146,** 590–620.

Chen, Y. J. & Morgan, W. J., 1990. A non-linear model for mid-ocean ridge axis tomography. *Journal of Geophysical Research* **95,** 17583–17604.

Chen, C.-H. & Presnall, D. C., 1975. The system $MgSiO_4$–SiO_2 at pressures up to 25 kilobars. *American Mineralogist* **60,** 398–406.

Cooper, R. F. & Kohlstedt, D. L., 1986. Rheology and structure of olivine-basalt partial melts. *Journal of Geophysical Research* **91,** 9315–9323.

Cordery, M. J. & Phipps Morgan, J., 1993. Convection and melting at mid-ocean ridges. *Journal of Geophysical Research* **98,** 19477–19503.

Cox, K. G., Smith, M. R. & Beswetherick, S., 1987. Textural studies of garnet lherzolites: evidence of exsolution origin from high-temperature harzburgites. In: Nixon, P. H. (ed.) *Mantle Xenoliths*. New York: John Wiley, pp. 537–550.

Detrick, R., Collins, J., Stenphen, R. & Swift, S., 1994. *In situ* evidence for the nature of the seismic layer 2/3 boundary in oceanic crust. *Nature* **370,** 288–290.

Dick, H. J. B., 1977*a*. Partial melting in the Josephine Peridotite; I, The effect on mineral composition and its consequence for geobarometry and geothermometry. *American Journal of Science* **277,** 801–832.

Dick, H. J. B., 1977*b*. Evidence of partial melting in the Josephine Peridotite. In: Dick, H. J. B. (ed.) *Magma Genesis, Proceedings of the American Geophysical Union Chapman Conference on Partial Melting in the Earth's Upper Mantle*, Portland, OR: Oregon Department of Geology and Mineral Industries, pp. 59–62.

Dick, H. J. B., 1989. Abyssal peridotites, very slow spreading ridges and ocean ridge magmatism. In: Saunders, A. D. & Norry, M. J. (eds) *Magmatism in the Ocean Basins. Geological Society Special Publication* **42,** 71–105.

Dick, H. J. B. & Fisher, R. L., 1984. Mineralogic studies of the residues of mantle melting: abyssal and alpine-type peridotites. In: Kornprobst, J. (ed.) *The Mantle and Crustal–Mantle Relationships—Mineralogical, Petrological, and Geodynamic Processes of the 3rd International Kimberlite Conference, Vol. II*. New York: Elsevier, pp. 295–308.

Dick, H. J. B. & Natland, J. H., 1996. Late-stage melt evolution and transport in the shallow mantle beneath the East Pacific Rise. In: Mével, C., Gills, K. M. & Allan, J. F. (eds) *Proceedings of the Ocean Drilling Program, 147*. College Station, TX: Ocean Drilling Program, pp. 103–134.

Dick, H. J. B., Fisher, R. L. & Bryan, W. B., 1984. Mineralogical variability of the uppermost mantle along mid-ocean ridges. *Earth and Planetary Science Letters* **69,** 88–106.

Elthon, D., 1989. Pressure of origin of primary mid-ocean ridge basalts. In: Saunders, A. D. & Norry, M. J. (eds) *Magmatism in the Ocean Basins. Geological Society Special Publication* **42,** 125–136.

Elthon, D., 1992. Chemical trends in abyssal peridotites: refertilization of depleted oceanic mantle. *Journal of Geophysical Research* **97,** 9015–9025.

Falloon, T. J. & Green, D. H., 1987. Anhydrous partial melting of MORB pyrolite and other peridotite compositions at 10 kbar: implications for the origin of MORB glasses. *Mineralogy and Petrology* **37,** 181–219.

Falloon, T. J. & Green, D. H., 1988. Anhydrous partial melting of peridotite from 8 to 35 kb and the petrogenesis of MORB. *Journal of Petrology, Special Lithosphere Issue* 379–414.

Falloon, T. J., Green, D. H., Hatton, C. J. & Harris, K. L., 1988. Anhydrous partial melting of a fertile and depleted peridotite from 2 to 30 kb and application to basalt petrogenesis. *Journal of Petrology* **29,** 1257–1282.

Forsyth, D. W., 1992. Geophysical constraints on mantle flow and melt generation beneath mid-ocean ridges. In: Phipps Morgan, J., Blackman, D. K. & Sinton, J. M. (eds) *Mantle Flow and Melt Generation at Mid-ocean Ridges. American Geophysical Union Monograph* **71,** 1–66.

Forsyth, D. W., 1993. Crustal thickness and the average depth and degree of melting in fractional melting models of passive flow beneath mid-ocean ridges. *Journal of Geophysical Research* **98,** 16073–16079.

Green, D. H. & Ringwood, A. E., 1967. The genesis of basaltic magmas. *Contributions to Mineralogy and Petrology* **15,** 103–190.

Hamlyn, P. R. & Bonatti, E., 1980. Petrology of mantle derived ultramafics from the Owen Fracture zone, Northwest Indian Ocean: implications for the nature of the oceanic upper mantle. *Earth and Planetary Science Letters* **48,** 65–79.

Hart, S. R. & Zindler, A., 1986. In search of bulk Earth composition. *Chemical Geology* **57,** 247–267.

Hékinian, R., Bideau, D., Cannat, M., Franchteau, J. & Hébert, R., 1992. Volcanic activity and crust–mantle exposure in the ultrafast Garret transform fault near 13°28′S in the Pacific. *Earth and Planetary Science Letters* **108,** 259–273.

Hékinian, R., Bideau, D., Franchteau, J., Cheminee, J. J., Armijo, R., Lonsdale, P. & Blum, N., 1993. Petrology of the East Pacific Rise crust and upper mantle exposed in Hess Deep (eastern equatorial Pacific). *Journal of Geophysical Research* **98,** 8069–8094.

Hékinian, R., Bideau, D., Herbért, R. & Niu, Y., 1995. Magmatism in the Garrett transform (East Pacific Rise near 13°27′S). *Journal of Geophysical Research* **100,** 10163–10185.

Hirose, K. & Kushiro, I., 1993. Partial melting of dry peridotites at high pressures: determination of compositions of melts segregated from peridotite using aggregates of diamonds. *Earth and Planetary Science Letters* **114,** 477–489.

Hirschmann, M. M. & Stolper, E. M., 1996. A possible role for garnet pyroxenite in the origin of the "garnet signature" in MORB. *Contributions to Mineralogy and Petrology* **124,** 185–209.

Hirth, G. & Kohlstedt, D. L., 1995. Experimental constraints on the dynamics of the partially molten upper mantle: deformation in diffusion creep regime. *Journal of Geophysical Research* **100,** 1981–2001.

Ito, G., Lin, J. & Gable, C. W., 1996. Dynamics of mantle flow and melting at a ridge-centered hotspot: Iceland and the Mid-Atlantic Ridge. *Earth and Planetary Science Letters* **144,** 53–74.

Ito, K. & Kennedy, G. C., 1967. Melting and phase relations in a natural peridotite to 40 kilobars. *American Journal of Science* **265,** 519–539.

Iwamori, H., 1994. ^{238}U–^{230}Th–^{226}Ra and ^{235}U–^{231}Pa disequilibria produced by mantle melting with porous and channel flows. *Earth and Planetary Science Letters* **125,** 1–16.

Jagoutz, E., Palme, H., Blum, H., Cendales, M., Dreibus, G., Spettel, B., Lorenz, V. & Wänke, H., 1979. The abundances of major, minor & trace elements in the earth's mantle as derived from primitive

ultramafic nodules. *Proceeding of 10th Lunar Planetary Science Conference. Geochimica et Cosmochimica Acta Supplement* **2,** 2031–2051.

Jamieson, B. G., 1970. Differentiation of ascending basic magma. In: Newwall, G. & Rast, N. (eds) *Mechanism of Igneous Intrusion. Geological Journal, Special Issue, No. 2* 165–176.

Jaques, A. L. & Green, D. H., 1980. Anhydrous melting of peridotite at 0–15 kb pressure and the genesis of tholeiitic basalts. *Contributions to Mineralogy and Petrology* **73,** 287–310.

Johnson, K. T. M. & Dick, H. J. B., 1992. Open system melting and the temporal and spatial variation of peridotite and basalt compositions at the Atlantis II F. Z. *Journal of Geophysical Research* **97,** 9219–9241.

Johnson, K. T. M., Dick, H. J. B. & Shimizu, N., 1990. Melting in the oceanic upper mantle: an ion microprobe study of diopside in abyssal peridotites. *Journal of Geophysical Research* **95,** 2661–2678.

Kelemen, P. B. & Dick, H. J. B., 1995. Focused melt flow and localized deformation in the upper mantle; juxtaposition of replacive dunite and ductile shear zones in the Josephine Peridotite, SW Oregon. *Journal of Geophysical Research* **100,** 423–438.

Kelemen, P. B., Joyce, D. B., Webster, J. D. & Holloway, J. R., 1990. Reaction between ultramafic rock and fractionating basaltic magma, II. Experimental investigations of reaction between olivine tholeiite and harzburgite at 1150–1050°C and 5 kb. *Journal of Petrology* **31,** 99–134.

Kelemen, P. B., Whitehead, J. A., Aharonov, E. & Jordahl, K. A., 1995*a*. Experiments on flow focusing in soluble porous media with applications to melt extraction from the mantle. *Journal of Geophysical Research* **100,** 475–496.

Kelemen, P. B., Shimizu, N. & Salters, V. J., 1995*b*. Extraction of mid-ocean-ridge basalt from the upwelling mantle by focused flow of melt in dunite channels. *Nature* **375,** 747–753.

Kinzler, R. J. & Grove, T. L., 1992. Primary magmas of mid-ocean ridge basalts, 2, applications. *Journal of Geophysical Research* **97,** 6907–6926.

Kinzler, R. J. & Grove, T. L., 1993. Corrections and further discussion of the primary magmas of mid-ocean ridge basalts, 1 and 2. *Journal of Geophysical Research* **98,** 22339–22347.

Klein, E. M. & Langmuir, C. H., 1987. Global correlations of ocean ridge basalt chemistry with axial depth and crustal thickness. *Journal of Geophysical Research* **92,** 8089–8115.

Klein, E. M. & Langmuir, C. H., 1989. Local versus global variation in ocean ridge basaltic composition: A reply. *Journal of Geophysical Research* **94,** 4241–4252.

Klein, E. M., Plank, T. & Langmuir, C. H., 1991. Constraints on models for mantle melting beneath ocean ridges. *RIDGE Events* **2,** 11–12.

Langmuir, C. H., 1995. Deep low F melts and the global systematics of MORB. *EOS Transactions of the American Geophysical Union* **76**(46), F694.

Langmuir, C. H., Klein, E. M. & Plank, T., 1992. Petrological systematics of mid-ocean ridge basalts: constraints on melt generation beneath ocean ridges. In: Phipps Morgan, J., Blackman, D. K. & Sinton, J. M. (eds) *Mantle Flow and Melt Generation at Mid-ocean Ridges. American Geophysical Union Monograph* **71,** 183–280.

Lesher, C. E. & Baker, M. B., 1996. Experimental partial melting of garnet lherzolite at 4 GPa: constraints on initial melting in plume environments. *EOS Transactions of the American Geophysical Union* **77**(46), F838.

Lundstrom, C. C., Shaw, H. F., Ryerson, F. J., Phinney, D. L., Gill, J. B. & Williams, Q., 1994. Compositional controls on the partitioning of U, Th, Ba, Pb, Sr, and Zr between clinopyroxene and haplobasaltic melts: implications for uranium series disequilibria in basalts. *Earth and Planetary Science Letters* **128,** 407–423.

Lundstrom, C. C., Gill, J. & Perfit, M. R., 1995. Mantle melting and basalt extraction by equilibrium porous flow. *Science* **270,** 1958–1961.

Maaløe, S., 1982. Geochemical aspects of permeability controlled partial melting and fractional crystallization. *Geochimica et Cosmochimica Acta* **46,** 43–57.

McDonough, W. F. & Sun, S.-s., 1995. The composition of the Earth. *Chemical Geology* **120,** 223–253.

McKenzie, D. P., 1967. Some remarks on heat flow and gravity anomalies. *Journal of Geophysical Research* **72,** 6261–6273.

McKenzie, D., 1984. The generation and compaction of partially molten rock. *Journal of Petrology* **25,** 713–765.

McKenzie, D., 1985*a*. ^{230}Th–^{238}U disequilibrium and the melting processes beneath ridge axes. *Earth and Planetary Science Letters* **72,** 137–152.

McKenzie, D., 1985*b*. The extraction of magma from the crust and mantle. *Earth and Planetary Science Letters* **79,** 81–91.

McKenzie, D. & Bickle, M. J., 1988. The volume and composition of melt generated by extension of the lithosphere. *Journal of Petrology* **29,** 625–679.

Michael, P. J. & Bonatti, E., 1985. Peridotite composition from the North Atlantic: regional and tectonic variations and implications for partial melting. *Earth and Planetary Science Letters* **73,** 91–l04.

Morgan, J. W., 1975. Heat flow and vertical movements of the crust. In: Fisher, A. G. & Judson, S. (eds) *Petroleum and Global Tectonics*. Princeton, NJ: Princeton University Press.

Mysen, B. O., 1979. Trace-element partitioning between garnet peridotite minerals and water-rich vapor: experimental data from 5 to 30 Kbar. *American Mineralogist* **64,** 274–287.

Natland, J. H., 1989. Partial melting of a lithologically heterogeneous mantle: inferences from crystallisation histories of magnesian abyssal tholeiites from the Siqueiros Fracture Zone. In: Saunders, A. D. & Norry, M. J. (eds) *Magmatism in the Ocean Basins. Geological Society Special Publication* **42,** 41–70.

Nicolas, A., 1986. A melt extraction model based on structural studies in mantle peridotites. *Journal of Petrology* **27,** 999–1022.

Nicolas, A., 1989. *Structures of Ophiolite and Dynamics of Oceanic Lithosphere*. Dordrecht: Kluwer Academic, 368 pp.

Niu, Y. & Batiza, R., 1991*a*. An empirical method for calculating melt compositions produced beneath mid-ocean ridges: application for axis and off-axis (seamounts) melting. *Journal of Geophysical Research* **96,** 21753–21777.

Niu, Y. & Batiza, R., 1991*b*. *In-situ* densities of silicate melts and minerals as a function of temperature, pressure, and composition. *Journal of Geology* **99,** 767–775.

Niu, Y. & Batiza, R., 1993. Chemical variation trends at fast and slow spreading ridges. *Journal of Geophysical Research* **98,** 7887–7902.

Niu, Y. & Batiza, R., 1994. Magmatic processes at the Mid-Atlantic Ridge ~26°S. *Journal of Geophysical Research* **99,** 19719–19740.

Niu, Y. & Batiza, R., 1997. Trace element evidence from seamounts for recycled oceanic crust in the eastern equatorial Pacific mantle. *Earth and Planetary Science Letters* **148,** 471–484.

Niu, Y. & Hékinian, R., 1997*a*. Spreading rate dependence of the extent of mantle melting beneath ocean ridges. *Nature* **385,** 326–329.

Niu, Y. & Hékinian, R., 1997*b*. Basaltic liquids and harzburgitic residues in the Garrett transform: a case study at fast-spreading ridges. *Earth and Planetary Science Letters* **146,** 243–258.

Niu, Y., Waggoner, D. G., Sinton, J. M. & Mahoney, J. J., 1996. Mantle source heterogeneity and melting processes beneath seafloor spreading centers: the East Pacific Rise, 18°–19°S. *Journal of Geophysical Research* **101,** 27711–27733.

Niu, Y., Langmuir, C. H. & Kinzler, R. J., 1997. Origin of abyssal peridotites: a new perspective. *Earth and Planetary Science Letters*, In press.

O'Hara, M. J., 1965. Primary magma and the origin of basalts. *Scottish Journal of Geology* **1,** 19–40.

O'Hara, M. J., 1968*a*. Are any ocean floor basalts primary magma? *Nature* **220,** 683–686.

O'Hara, M. J., 1968*b*. The bearing of phase equilibria studies in synthetic and natural systems on the origin and evolution of basic and ultrabasic rocks. *Earth-Science Reviews* **4,** 69–133.

Oxburgh, E. R., 1980. Heat flow and magma genesis. In: Hargraves, R. B. (ed.) *Physics of Magmatic Processes*. Princeton, NJ: Princeton University Press, pp. 161–199.

Parmentier, E. M. & Phipps Morgan, J., 1990. The spreading rate dependence of three-dimensional spreading center structure. *Nature* **348,** 325–328.

Parsons, B. & Sclater, J. G., 1977. An analysis of the variation of ocean floor bathymetry with age. *Journal of Geophysical Research* **82,** 803–827.

Phipps Morgan, J., 1987. Melt migration beneath mid-ocean ridge spreading centres. *Geophysical Research Letters* **14,** 1238–1241.

Phipps Morgan, J. & Forsyth, D. W., 1988. Three-dimensional flow and temperature perturbations due to a transform offset: effect on oceanic crustal and upper mantle structure. *Journal of Geophysical Research* **93,** 2955–2966.

Plank, T. & Langmuir, C. H., 1992. Effects of the melting regime on the composition of the oceanic crust. *Journal of Geophysical Research* **97,** 19749–19770.

Plank, T., Spiegelman, M., Langmuir, C. H. & Forsyth, D. W., 1995. The meaning of 'mean F': clarifying the mean extent of melting at ocean ridges. *Journal of Geophysical Research* **100,** 15045–15052.

Presnall, D. C, Dixon, T. H., O'Connell, T. H. & Dixon, S. A., 1979. Generation of mid-ocean ridge tholeiites. *Journal of Petrology* **20,** 3–35.

Prinz, M., Keil, K., Green, J. A., Reid, A. M., Bonatti, E. & Honnorez, J., 1976. Ultramafic and mafic dredge samples from the equatorial Mid-Atlantic Ridge and fracture zones. *Journal of Geophysical Research* **81,** 4087–4103.

Prinzhofer, A. & Allègre, C. J., 1985. Residual peridotites and the mechanisms of partial melting. *Earth and Planetary Science Letters* **74,** 251–265.

Qin, Z., 1992. Disequilibrium partial melting model and its implications for trace element fractionations during mantle melting. *Earth and Planetary Science Letters* **112,** 75–90.

Reid, I. & Jackson, H. R., 1981. Oceanic spreading rate and crustal thickness. *Marine Geophysical Research* **5,** 165–172.

Ribe, N. M., 1996. The dynamics of plume–ridge interaction 2, Off-axis plumes. *Journal of Geophysical Research* **101,** 16195–16204.

Riley, G. N. & Kohlstedt, D. L., 1990. An experimental study of melt migration in an olivine–melt system. In: Ryan, M. P. (ed.) *Magma Transport and Storage*. New York: John Wiley, pp. 77–86.

Roeder, P. L. & Emslie, R. F., 1970. Olivine–liquid equilibrium. *Contributions to Mineralogy and Petrology* **29,** 275–289.

Rubin, K. H. & Macdougall, J. D., 1988. ^{226}Ra excesses in mid-ocean ridge basalts and mantle melting. *Nature* **335,** 158–161.

Rubin, K. H. & Macdougall, J. D., 1990. Dating of neovolcanic MORB using (^{226}Ra/^{230}Th) disequilibrium. *Earth and Planetary Science Letters* **101,** 313–322.

Salters, V. J. M., 1996. The generation of mid-ocean ridge basalts from the Hf and Nd isotope perspective. *Earth and Planetary Science Letters* **141,** 109–123.

Salters, V. J. M. & Hart, S. R., 1989. The hafnium paradox and the role of garnet in the source of mid-ocean ridge basalts. *Nature* **342,** 420–422.

Schilling, J.-G., 1991. Fluxes and excess temperatures of mantle plumes inferred from their interaction with migrating mid-ocean ridges. *Nature* **352,** 397–403.

Scott, D. R. & Stevenson, D. J., 1989. A self-consistent model of melting, magma migration and buoyancy-driven circulation beneath mid-ocean ridges. *Journal of Geophysical Research* **94,** 2973–2988.

Shen, Y. & Forsyth, D. W., 1995. Geochemical constraints on initial and final depth of melting beneath mid-ocean ridges. *Journal of Geophysical Research* **100,** 2211–2237.

Sinton, J. M. & Detrick, R. S., 1992. Mid-ocean ridge magma chambers. *Journal of Geophysical Research* **97,** 197–216.

Sleep, N. H., 1988. Tapping of melts by veins and dykes. *Journal of Geophysical Research* **93,** 10255–10272.

Snow, J. E. & Dick, H. J. B., 1995. Pervasive magnesium loss by marine weathering of peridotite. *Geochimica et Cosmochimica Acta* **59,** 4219–4235.

Sparks, D. W. & Parmentier, E. M., 1991. Melt extraction from the mantle beneath spreading centres. *Earth and Planetary Science Letters* **105,** 368–377.

Spiegelman, M. & Elliot, T., 1993. Geochemical consequences of magma transport for U-series disequilibrium. *Earth and Planetary Science Letters* **118,** 1–20.

Spiegelman, M. & Kenyon, P., 1992. The requirements for the chemical disequilibrium during magma migration. *Earth and Planetary Science Letters* **109,** 611–620.

Spiegelman, M. & McKenzie, D., 1987. Simple 2-D models for melt extraction at mid-ocean ridges and island arcs. *Earth and Planetary Science Letters* **83,** 137–152.

Stevenson, D. J., 1989. Spontaneous small-scale melt segregation in partial melts undergoing deformation. *Geophysical Research Letters* **16,** 1067–1070.

Stolper, E., 1980. A phase diagram for mid-ocean ridge basalts: preliminary results and implications for petrogenesis. *Contributions to Mineralogy and Petrology* **74,** 13–27.

Stolper, E., Walker, D., Hager, B. H. & Hays, J. F., 1981. Melt segregation from partially molten source region, the importance of melt density and source region size. *Journal of Geophysical Research* **86,** 6261–6271.

Turcotte, D. L. & Phipps Morgan, J., 1992. Magma migration and mantle flow beneath a mid-ocean ridge. In: Phipps Morgan, J., Blackman, D. K. & Sinton, J. M. (eds) *Mantle Flow and Melt Generation at Mid-ocean Ridges. American Geophysical Union Monograph* **71,** 155–182.

Walker, D., Shibata, T. & DeLong, S. E., 1979. Abyssal tholeiites from the Oceanographer Fracture Zone, II, Phase equilibria and mixing. *Contributions to Mineralogy and Petrology* **70,** 111–125.

Walter, M. J. & Presnall, D. C., 1994. Melting behavior of simplified lherzolite in the system CaO–MgO–Al_2O_3–SiO_2–Na_2O from 7 to 35 kbar. *Journal of Petrology* **35,** 329–359.

Walter, M. J., Sisson, T. W. & Presnall, D. C., 1995. A mass proportion method for calculating melting reactions and application to melting of model upper mantle lherzolite. *Earth and Planetary Science Letters* **135,** 77–90.

Wood, B. J., 1987. Thermodynamics of multiple component systems containing several solid solutions. In: Carmichael, I. S. E. & Eugster, H. P. (eds) *Thermodynamic Modelling of Geological Materials: Minerals, Fluids and Melts. Mineralogical Society of America, Reviews in Mineralogy* **17,** 71–96.

Zhang, Y.-S. & Tanimoto, T., 1993. High resolution global upper mantle structure and plate tectonics. *Journal of Geophysical Research* **98,** 9793–9823.

APPENDIX A

Table A1: Expressions of the bulk distribution coefficients for mNB91

D_{SiO_2}	=	0·8480	−	0·2200F	+	0·0055P		
D_{TiO_2}	=	0·1064	−	0·0075F	+	$1{\cdot}3236 \times 10^{-4}F^2$		
$D_{Al_2O_3}$	=	0·1890	−	0·5100F	−	$2{\cdot}5 \times 10^{-4}F^{-1}$	+ 0·0010P	
D_{FeO}	=	0·3169	+	0·3695F	−	$3{\cdot}4586 \times 10^{-3}P$	+ 0·2130D_{MgO}	
D_{MgO}	=	5·2000	−	7·5664F	−	0·0594P		
D_{CaO}	=	0·3180	−	1·2200F	+	$2{\cdot}7200 \times 10^{-3}F^{-1}$	+ 0·0005P	
D_{Na_2O}	=	0·0639	−	0·5787F	+	2·4763F^2	−3·6717F^3	

The empirical model NB91 (Niu & Batiza, 1991*a*) was built on experimental data by Jaques & Green (1980), Falloon & Green (1987, 1988) and Falloon *et al.* (1988). The modified NB91, called mNB91, incorporates recent data of peridotite melting experiments conducted using diamond aggregates technique by Hirose & Kushiro (1993) and Baker & Stolper (1994). In these expressions, F is the extent of melting as mass fractions, and P is pressure in kilobars.

APPENDIX B

Table B1: Comparison of the preferred source with other commonly used fertile mantle compositions

	HZ86	MS95	J.79	BS94	FG87	HK93	PS
SiO_2	45·96	45·00	45·16	45·50	44·74	44·48	45·50
TiO_2	0·18	0·20	0·22	0·11	0·17	0·16	0·16
Al_2O_3	4·06	4·45	3·97	3·98	4·37	3·59	4·20
Cr_2O_3	0·47	0·38	0·46	0·68	0·45	0·31	0·45
FeO	7·54	8·05	7·82	7·18	7·55	8·10	7·70
MnO	0·13	0·14	0·27	0·13	0·11	0·12	0·13
MgO	37·80	37·80	38·30	38·30	38·57	39·22	38·33
CaO	3·21	3·55	3·50	3·57	3·38	3·44	3·40
NiO	0·28		0·27	0·23	0·26	0·25	0·26
Na_2O	0·33	0·36	0·33	0·31	0·40	0·30	0·30
K_2O	0·03	0·03	0·03		0·03	0·02	
mg-no.	89·94	89·33	89·72	90·48	90·11	89·62	89·87
CaO/Al_2O_3	0·79	0·80	0·88	0·90	0·77	0·96	0·81

HZ86 is the primitive upper mantle of Hart & Zindler (1986); MS95 is the primitive mantle (or bulk silicate Earth) of McDonough & Sun (1995); J.79 is the model mantle composition of Jagoutz *et al.* (1979); BS94 is the model composition MM3 of Baker & Stolper (1994); FG87 is the MORB pyrolite 90 of Falloon & Green (1987); HK93 is KLB-1, a less fertile peridotite thought to be more appropriate for MORB mantle, used in melting experiments by Hirose & Kushiro (1993). PS is the preferred source used in this study, which is within the range of suggested mantle compositions in the literature with values chosen to be consistent with the abyssal peridotite data, and recognizing that the MORB source must be depleted in incompatible elements (e.g. lower TiO_2 and Na_2O, and slightly higher CaO/Al_2O_3 than estimated primitive mantle).

APPENDIX C

Table C1: Conversion of CIPW norms to mantle normative mineralogies

CIPW norms calculated from bulk-rock data
Ab = $NaAlSi_3O_8$
An = $CaAl_2Si_2O_8$
Di = $(Ca,Mg,Fe)_2Si_2O_6$
Hy = $(Mg,Fe)_2Si_2O_6$
Ol = $(Mg,Fe)_2SiO_4$
Conversions
Jd ($NaAlSi_2O_6$) = Ab − SiO_2
Ca-Ts ($CaAl_2SiO_6$) = An − SiO_2
Hy = Ol + SiO_2
Normative minerals of peridotites
Ol [$(Mg,Fe)_2SiO_4$] = Ol − Ab − An
Opx [$(Mg,Fe)_2SiO_4$] = Hy + Ab + An
Cpx [(Na,Ca)(Fe,Mg,Al)(Al,$Si)_2O_6$] = Di + Ab + An

Ab, albite; An, anorthite; Di, diopside; Hy, hypersthene (Opx); Ol, olivine; Jd, jadeite (Cpx); Ca-Ts, calcium Tschermakite (Cpx); Ol, olivine, Opx, orthopyroxene; Cpx, clinopyroxene.

APPENDIX D

Similiar to Fig. 12, but constructed before removing the excess olivine to show that *opx* − *F* has a greater slope (0·702) than *cpx* − *F* (0·452), indicating that equation (8) is not an artefact of calculations, but a true signature of abyssal peridotites, and is consistent with polybaric melting reactions [see Fig. 8b, and equations (1) and (5)–(8)].

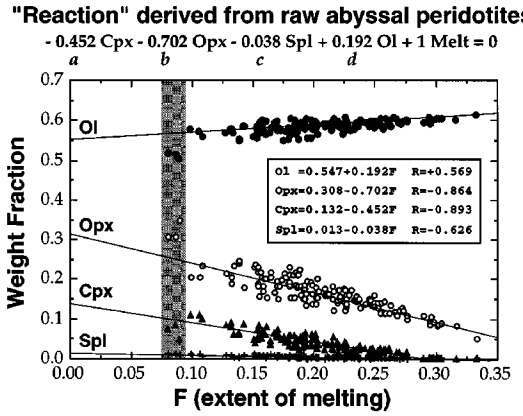

APPENDIX E

Table E1: Summary of data and model results

	Vulcan FZ	A II FZ E Wall	Islas Orcadas FZ	A II FZ W Wall	Bullard FZ	Bouvet FZ	Whole data set
Average modes in abyssal peridotites (vol. %)							
Ol	70·14	68·90	72·58	70·98	75·41	81·26	72·93
1σ	3·87	9·41	4·80	12·60	4·05	4·00	8·19
Opx	21·00	23·52	21·83	22·74	19·42	16·17	21·09
1σ	2·85	6·52	3·50	7·44	2·93	3·22	5·28
Cpx	7·84	6·68	4·77	4·66	4·49	1·91	5·00
1σ	2·44	3·47	2·22	5·55	2·20	1·35	3·58
Spl	1·01	0·68	0·73	0·50	0·59	0·46	0·68
1σ	0·34	0·22	0·34	0·28	0·28	0·26	0·35
Excess Ol and 'excess' Opx (wt %)							
Ol	22·53	26·88	26·44	32·57	29·38	39·37	29·09 (32·66)
1σ	8·53	10·12	9·50	9·53	13·20	8·43	11·31 (11·39)
Opx	−1·36	0·31	0·07	0·78	−0·08	−0·01	0·06 (1·18)
1σ	1·31	1·16	1·09	1·03	1·37	1·56	1·38 (0·06)
Average modes in melting residues (wt %)							
Ol	59·46	62·30	63·07	64·40	65·70	69·69	64·09 (62·39)
1σ	3·51	2·66	3·55	4·50	3·71	4·14	4·80 (6·26)
Opx	29·79	28·60	29·09	28·82	26·92	25·92	28·27 (29·51)
1σ	2·70	1·53	2·70	2·85	2·46	2·90	2·91 (4·56)
Cpx	9·61	8·31	7·02	6·17	6·68	3·82	6·87 (6·83)
1σ	2·22	2·28	2·15	2·35	2·19	1·93	2·74 (3·41)
Spl	1·14	0·79	0·82	0·61	0·70	0·57	0·77 (1·03)
1σ	0·35	0·24	0·33	0·30	0·32	0·30	0·36 (0·53)
Melting modes (in weight fraction)							
aCpx + bOpx + cSpl + dOl + 1Melt = 0							
Ol (d)	0·2125	0·0365	0·1684	0·1443	0·0560	0·1100	0·1667 (0·1933)
SE	0·0968	0·1598	0·0701	0·0487	0·0716	0·0789	0·0256
Opx (b)	−0·6095	−0·3517	−0·6492	−0·6974	−0·5696	−0·7157	−0·6517 (–0·6813)
SE	0·1735	0·2294	0·1103	0·0852	0·1248	0·1188	0·0438
Cpx (a)	−0·5270	−0·6357	−0·4823	−0·4190	−0·4546	−0·3608	−0·4657 (–0·4640)
SE	0·1007	0·1086	0·0578	0·0424	0·0647	0·0598	0·0227
Spl (c)	−0·0760	−0·0490	−0·0368	−0·0279	−0·0317	−0·0335	−0·0492 (–0·0480)
SE	0·0208	0·0278	0·0193	0·0124	0·0154	0·0194	0·0057
Mean extent of melting and mean equilibration pressure							
F_M	0·104	0·133	0·144	0·161	0·169	0·215	0·154 (0·154)
1σ	0·035	0·033	0·035	0·046	0·039	0·038	0·050
P_M (kbar)	12·4	18·9	12·5	12·5	18·7	14·7	15 (14)
1σ	2	2	2	2	2	2	5

All the calculations are done based on the preferred mantle source composition (Appendix B) with MgO = 38·33 wt %. F values used in all calculations are derived from the regression equation in Fig. 5c. The values in parentheses for the entire data set are derived by using a source composition similar to HZ86 with MgO = 37·8 wt % (Appendix B). The F values used in these calculations are derived from $F = -1·232 + 0·03271$MgO. The melting modes for the entire data set are statistically more representative of melting residues beneath ocean ridges than individual suites (determined by fewer data points), and can be used for trace element modelling.